Bioconjugate Chemistry

pubs.acs.org/bc Review

Fluorescent Bioconjugates for Super-Resolution Optical Nanoscopy

30th Anniversary Review

Zhihe Liu, Jie Liu, Xiaodong Wang, Feixue Mi, Dan Wang, and Changfeng Wu*

Cite This: *Bioconjugate Chem.* 2020, 31, 1857−1872 Read Online

ABSTRACT: Fluorescent microscopy techniques are widely used in biological studies. However, the spatial resolution of fluorescent microscopy is restricted by the optical diffraction limit. In the past two decades, super-resolution imaging techniques with different principles have been invented to visualize biomolecules at nanometer scales. The development of nearly all these techniques is closely related to the advances in fluorescent probes. In particular, the intrinsic properties of fluorescent probes constrain the optimal imaging performance of super-resolution nanoscopy techniques. In this review, we summarized the recent progress in fluorescent probe bioconjugates for super-resolution imaging techniques. Examples of these bioconjugates include the widely used fluorescent proteins (FPs), organic dyes, quantum dots (Qdots), carbon dots (Cdots), upconversion nanoparticles (UCNPs), aggregation induced emission (AIE) nanoparticles, and polymer dots (Pdots). Based on the characteristics of the existing probes and their adaptability in current imaging methods, we provide a perspective for further development of fluorescent probes for super-resolution imaging.

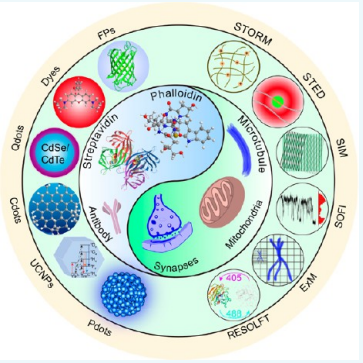

1. INTRODUCTION

Direct visualization of subcellular structures and dynamic processes, such as protein−protein interactions, the symbiotic relationship of organelles and quantification of components, is crucial for biology studies.[1−3] To obtain this biological information, researchers have invented a variety of imaging techniques, including transmission electron microscopy (TEM), cryo-electron microscopy (cryo-EM), and fluorescent microscopy. By virtue of the high contrast achieved by the proper staining process, we can visualize subcellular organelles inside live cells by fluorescence microscopy. It has become the most powerful technique in cell biology and biomedicine.[4−7] However, the spatial resolution of conventional fluorescence microscopy is constrained by the optical diffraction limit (∼200 nm) even though an objective with high numerical aperture (∼1.5) was equipped. The diffraction-limited resolution hindered the performance of optical microscopy for over a century and restricted the ability of optical instruments to distinguish subcellular structures and dynamic processes at nanometer scales.

Optical nanoscopy has revolutionized the study of subcellular architecture and dynamics and is on its way to becoming the new gold standard in fluorescence imaging.[8−11] To date, different types of super-resolution fluorescence microscopy have been invented and widely used in biological studies. According to the working principles, super-resolution fluorescent imaging can be categorized into four types: (i) point spread function (PSF) modulated super-resolution nanoscopy, including stimulated emission depletion fluorescence nanoscopy (STED),[12−19] structured illumination microscopy (SIM),[20−25] ground state depletion (GSD),[26−28] and reversible saturable optical linear fluorescence transitions (RESOLFT);[29−34] (ii) single molecule localization based super-resolution nanoscopy (SMLM), including stochastic optical reconstruction microscopy (STORM),[35−45] photoactivated localization microscopy (PALM);[46−53] (iii) fluorescent probe fluctuation based super-resolution nanoscopy, including super-resolution optical fluctuation imaging (SOFI),[54−64] Bayesian analysis of the blinking and bleaching (Three B),[65,66] super-resolution radial fluctuations (SRRF);[67] (iv) sample expansion based super-resolution nanoscopy, which is called expansion microscopy (ExM).[68−73] Except for SIM, all of these super-resolution imaging techniques are dependent on the photophysical properties of fluorescent probes. Each super-resolution technique shows specific advantages and drawbacks in imaging performance. The spatial resolution and temporal resolution are a pair of tradeoff factors in super-resolution imaging techniques. The spatial resolution of SMLM based nanoscopy is high while using excellent photoswitchable probes. However, the temporal resolution of SMLM is decreased by capturing more than thousand frames

Received: May 28, 2020
Revised: July 8, 2020
Published: July 10, 2020

https://dx.doi.org/10.1021/acs.bioconjchem.0c00320
Bioconjugate Chem. 2020, 31, 1857−1872

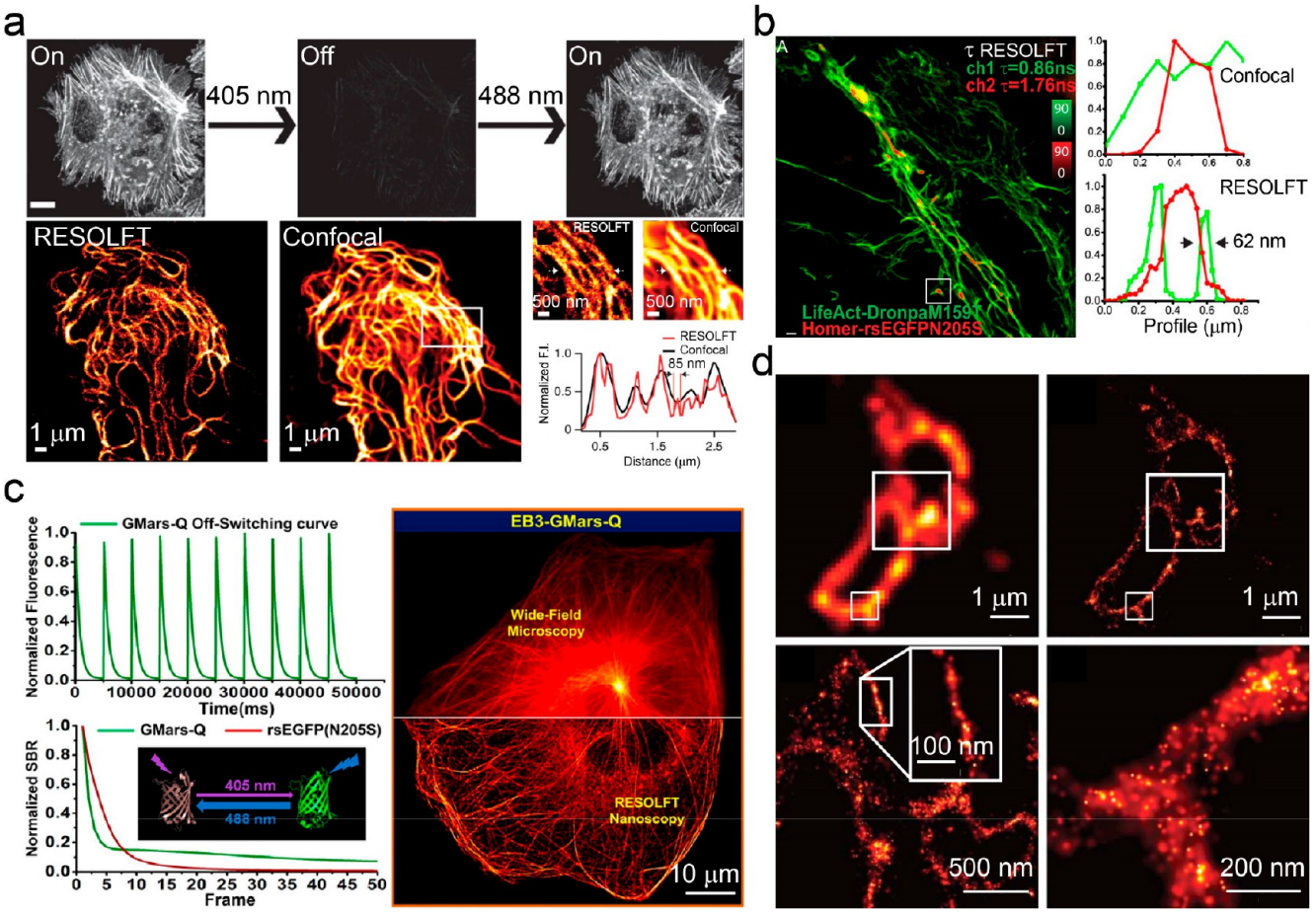

Figure 1. Fluorescent proteins for super-resolution nanoscopy. (a) Repeated photoswitching of β-actin-Kohinoor expressed in live HeLa cells and RESOLFT imaging of a live HeLa cell expressing vimentin-Kohinoor. Adapted with permission from ref 31, Copyright 2015, Nature Publishing Group. (b) Dual channel τ-RESOLFT image of DronpaM159T labeled lifeAct and rsEGFPN205S labeled homer in brain tissue. The line profiles quantified the improvement of spatial resolution of τ-RESOLFT. Adapted with permission from ref 32, Copyright 2014, American Chemical Society. (c) Characterization of GMars-Q FP and comparison of wide field image with RESOLFT of cytoskeleton structures in U2OS cell. Adapted with permission from ref 29, Copyright 2016, American Chemical Society. (d) Comparison of total internal reflection fluorescence microscopy and PALM nanoscopy images of cryo-prepared thin section of COS-7 cell expressing Kaede tagged lysosomal transmembrane protein CD63. Adapted with permission from ref 46. Copyright 2006, American Association for the Advancement of Science.

of image sequences. PSF modulated super-resolution nanoscopy, such as STED and GSD, usually shows better temporal resolution as compared with SMLM techniques. However, the spatial resolution is dependent on the intensity of depletion laser. The biosamples can be destroyed by the high intensity laser illumination. Generally, SOFI, Three B, and SRRF show a balanced spatial−temporal resolution by capturing time-dependent frame sequences. However, all these blinking based nanoscopy techniques need plenty of computing power for reconstruction of super-resolution images from the image sequences. The ExM technique shows advantages in image acquisition by conventional microscopy. However, the sample expansion including multiple tedious steps, suffer from fluorophore degradation, and is not suitable for living cell imaging.

The performance of the super-resolution fluorescence imaging techniques is largely dependent on the optical properties of the fluorescent probes. A new imaging technique usually poses different photophysical challenges for fluorescent probes, including the absorption cross sections, fluorescence quantum yields, excited state lifetimes, photostability, stimulation−depletion properties, photoswitchable properties, and photoblinking properties. Fluorescent probes can be classified into endogenic and exogenous probes. Endogenic fluorescent probes mainly refer to fluorescent proteins, which can be transfected and synthesized intracellularly with specific protein expression. For exogenous fluorescent probes, there are biocompatible small molecule organic dyes and nanomaterials that including quantum dots (Qdots), carbon dots (Cdots), upconversion nanoparticles (UCNPs), aggregation induced emission (AIE) nanoparticles, and polymer dots (Pdots). In this review, we discuss the fluorescent probe bioconjugates that are suitable for super-resolution imaging. Particularly, we aim to highlight the newly developed fluorescent probes and discuss their photophysical properties required for further development of the super-resolution nanoscopy.

2. ENDOGENIC FLUORESCENT PROBES FOR SUPER-RESOLUTION NANOSCOPY

Fluorescent proteins (FPs) are a series of proteins that can be expressed intracellularly and modified by changing amino acid sequences.[74−76] The application of FPs in super-resolution imaging techniques has revolutionized cell biology.[77,78] Hell et al. transfected pQE30-asFP595 plasmid and expressed asPF595

https://dx.doi.org/10.1021/acs.bioconjchem.0c00320
Bioconjugate Chem. 2020, 31, 1857−1872

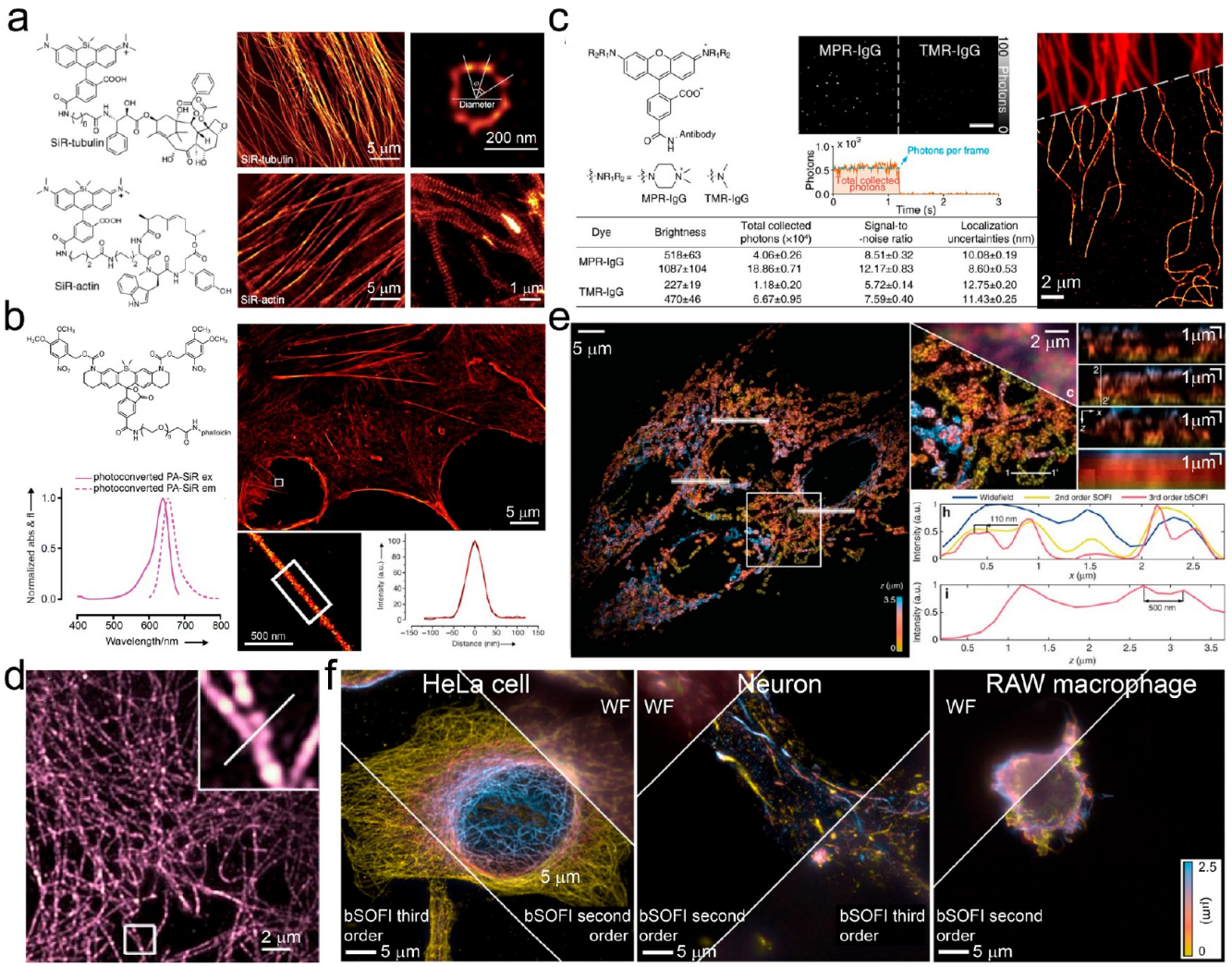

Figure 2. Organic dyes for super-resolution nanoscopy. (a) Chemical structures of SiR-tubulin and SiR-actin. SIM images of SiR-tubulin and SiR-actin labeled human fibroblasts (middle panel); STED image (deconvoluted by Richardson-Lucy algorithm) of SiR-tubulin labeled centrosomal microtubules (right up-panel); STED image (raw data) of SiR-actin labeled axons of rat primary hippocampal neurons (lower-right panel). Adapted with permission from ref 85, Copyright 2014, Nature Publishing Group. (b) Chemical structure and spectrum of phalloidin conjugated PA-SiR. PALM images of phalloidin conjugated PA-SiR labeled actin in COS-7 cells and line-scan intensity across filopodial structure (fwhm = 45 nm). Adapted with permission from ref 91, Copyright 2016, John Wiley and Sons. (c) Chemical structures and characterizations of MPR-IgG and TMR-IgG. Comparison of wide-field and PALM image of MPR-IgG labeled α-tubulin. Adapted with permission from ref 94, Copyright 2019, American Chemical Society. (d) SOFI image of Alexa 647 immunolabeled β-tubulin network of COS-7 cells. Adapted with permission from ref 101, Copyright 2010, John Wiley and Sons. (e) Depth encoded 3D-SOFI nanoscopy images of Alexa647 labeled mitochondria in fixed C2C12 cells (left panel). Enlarged region and line-scan profiles of lateral and axial resolution with widefield, second-order SOFI and third-order SOFI, respectively (right panel). Adapted with permission from ref 103, Copyright 2014, Nature Publishing Group. (f) Multiphase retrieval combined 3D-balanced SOFI images of Alexa 647 labeled microtubule in HeLa cells, mouse hippocampal primary neurons, and RAW macrophage. Adapted with permission from ref 104, Copyright 2018, Nature Publishing Group.

protein in the bacteria *Escherichia coli*. Using asPF595 protein, they demonstrated the concept of RESOLFT super-resolution imaging technique and obtained about 90 nm spatial resolution.[33] Nagai et al. developed a Kohinoor fluorescent protein, which is fast-switching and positively photoswitchable. As shown in Figure 1a, they applied Kohinoor in RESOLFT nanoscopy and obtained about 85 nm resolution of vimentin in living HeLa cells with ultralow laser intensity (0.004 J/cm^2).[31] To dynamically observe subcellular organelles, Hell et al. introduced a time correlated single photon counting card into traditional RESOLFT and invented dual channel modality τ-RESOLT nanoscopy.[32] They developed two types of reversibly switchable fluorescent proteins (rsFPs), named DronpaM159T and rsEGFPN205S. The spatial resolution was improved to about 62 nm in living brain tissue (Figure 1b).[32]

To improve the photophysical properties of FPs in RESOLFT nanoscopy, Sun et al. developed a monomeric rsFP termed GMars-Q, which shows low residual off-state fluorescence and high photostability (Figure 1c).[29] They achieved parallelized RESOLFT nanoscopy imaging of a variety of subcellular organelles, such as endoplasmic reticulum, microtubules, intermediate filaments, and the Golgi complex in mammalian cells. Furthermore, they developed GMars-T rsFP with their photophysical properties suitable for both RESOLFT and SOFI nanoscopy, and demonstrated about 80 nm spatial resolution of microtubules in U2OS cell.[79] With regard to rsFPs, Xu et al. developed a

https://dx.doi.org/10.1021/acs.bioconjchem.0c00320
Bioconjugate Chem. 2020, 31, 1857−1872

monomeric green rsFP Skylan-S, which shows high photostability and an improved fluorescence fluctuation suitable for higher-order SOFI nanoscopy.[80] Super-resolution imaging of Skylan-S labeled tubulin structures and clathrin-coated pits (CCPs) in living U2OS cells was demonstrated by third-order SOFI nanoscopy and a ∼90 nm resolution of CCPs structure was obtained.[80]

In 2006, Betzig et al. invented PALM technique and initially applied photoactivatable fluorescent protein (PAFP) in this super-resolution imaging technology. PALM is dependent on sparsely distributed fluorescent signals collected from each photoactive probe within a diffraction-limited region. Combining with single-particle localization and image-stacking algorithms, the precise location of an individual molecule can be extracted and reconstructed. They chose tetrameric Kaede and oligomers of EosFP PAFPs for functional subcellular structure imaging.[46] By fusing PAFP Kaede with the lysosomal transmembrane protein CD63 in COS-7 cells, they obtained PALM images with about 10 nm resolution and revealed small associated membranes that may represent interacting between lysosomes and late endosomes (Figure 1d). Dedecker et al. developed a green-to-red photoconvertible Dronpa FPs with high brightness, low photobleaching, and distinct photoblinking by using evolutionary and structure-driven design strategy.[81] One of the screened Dronpa mutants, pcDronp2, was tagged to human β-actin in HeLa cells and applied in PALM and SOFI imaging techniques. Furthermore, they developed enhanced fluorescence GFP with higher expression levels and obtained ∼70 nm spatial resolution of vimentin in living HeLa cells.[82] Xu et al. developed Quick-SIMBA, a high temporal−spatial resolution nanoscopy that combined single molecule localization microscopy with Bayesian localization microscopy.[83] Combined with a newly developed photoconvertible FP, pcStar, they revealed a specific "parallel three-pillar" structure of the neuronal−glial cell junction in *Drosophila* embryos.[83]

Boyden et al. developed protein-retention expansion microscopy (proExM) that use genetically encoded fluorescent proteins to visualize cytoskeletal structures and mammalian brain circuitry on conventional diffraction-limited microscope. Various fluorescent proteins with emission spectra ranging from blue to near-infrared, such as mEmerald, EYFP, and mRuby2, were examined to report signals in the proExM workflow. However, the fluorescence retention after sample expansion is ∼50% of their initial fluorescence intensity.[84] Similarity, Vaughan et al. used GFP, YFP, and Ds-red fusion protein to reveal nanoscale intracellular structures in cultured cells and mouse brain tissue, which represented the rapid dissemination of ExM technology.[70] The endogenous fluorescent proteins exhibited unique advantages for living cell super-resolution imaging. However, the fluorescent brightness and photostability are still key limitations for long-term dynamic imaging.

3. EXOGENOUS FLUORESCENT PROBES FOR SUPER-RESOLUTION NANOSCOPY

3.1. Small Molecule Organic Dyes (Dyes). Organic dyes with different properties and functions were extensively used in super-resolution nanoscopy and biological studies. Here, we focus on some representative dyes with improved photophysical properties in recent years. To avoid the green autofluorescence generated from biological samples when excited by UV or blue light, red-emissive dyes are often better choices. Rhodamine dyes have long been recognized as a great framework for building small molecule probes, as the rhodamines show excellent quantum yields. Recently, rhodamine and its derivatives were modified to apply in super-resolution imaging. Johnsson et al. designed and synthesized two types of silicon containing rhodamine (Silicon−Rhodamine, SiR) derivates with tubulin and actin targeting functions, called SiR-tubulin and SiR-actin (Figure 2a).[85] Both of these SiR dyes show far-red emission, excellent brightness, photostability, and efficient subcellular labeling capability. As demonstrated in STED nanoscopy, the ring of the centrosomal microtubules along the longitudinal axis was resolved in living human fibroblasts and the polar angle between two neighboring centrioles is about 39° ± 13°. In addition, the actin rings labeled with SiR-actin in hippocampal neurons are observed with unprecedented resolution.[85] By conjugation Si-Rhodamine with a commercial DNA-targeted dye Hoechst 33342, they achieved live-cell nuclei super-resolution imaging.[86] In STED nanoscopy, 660 and 775 nm depletion lasers are advantageous, as they cause less autofluorescence and photobleaching. Hell et al. developed a series of orange-red emission (618 nm) membrane-permeant rhodamine-based fluorescent probes for single- and dual-color STED nanoscopy in living HeLa cells. About 40−60 nm spatial resolution was obtained.[87] Furthermore, they synthesized functionalized SiR probes with large Stokes shift and emission spectrum ranging from 650 to 700 nm and demonstrated multicolor STED nanoscopy in living cells.[88−90]

SiR dyes show great potential for several super-resolution imaging techniques. Besides the STED nanoscopy, SiR dye and its derivates have also been widely used in SMLM. Lavis et al. synthesized a photoactivatable SiR dye (PA-SiR) by changing N-substitution patterns and replacing the xanthene oxygen with a dimethylsilicon moiety to shift the maxima absorption and emission to longer wavelength (Figure 2b).[91] The chemical structure indicated that acylation of the rhodamine nitrogen atoms leads the PA-SiR to a nonfluorescent lactone form. They demonstrated PALM imaging of COS-7 cell with phalloidin conjugated PA-SiR. The spatial resolution of PA-SiR labeled F-actin is about 45 nm with 5.3 nm localization precision.[91] Rivera-Fuentes et al. synthesized a photoactivatable rhodamine derivative probe for which fluorescent response depends on esterase activity.[92] This study introduced a mechanism for enzymatic activity sensing in living cells using PALM nanoscopy.[92] The on-time photochromic switching is one of the key characteristics for fluorescent probes in SMLM. Xiao et al. developed photochromic rhodamine dyes with long-term on-time switching by installing a carboxyl group close to the lactam site in rhodamine structures to improve the intramolecular acidic environment, thus stabilizing the photoactivated zwitterionic structure.[93] As shown in Figure 2c, Xiao et al. developed a quanternary piperazine-substituted rhodamine (MPR) probe to alleviate the brightness loss caused by twisted intramolecular charge transfer (TICT) upon photoexcitation. They introduced a quaternary piperazine moiety to replace the dimethylamino group in tetramethyl rhodamine (TMR). The electronic inductive effect resulted in about 0.93 quantum yield of MPR, which is 2-fold brighter than TMR. By conjugation with IgG, MPR-IgG show significant improvements in single particle brightness and localization precision (10.08 ± 0.19 nm). In PALM nanoscopy, MPR-IgG labeled microtubules in HeLa cells revealed refined structures as compared with conventional wide-field microscopy.[94] Tetin et

https://dx.doi.org/10.1021/acs.bioconjchem.0c00320
Bioconjugate Chem. 2020, 31, 1857−1872

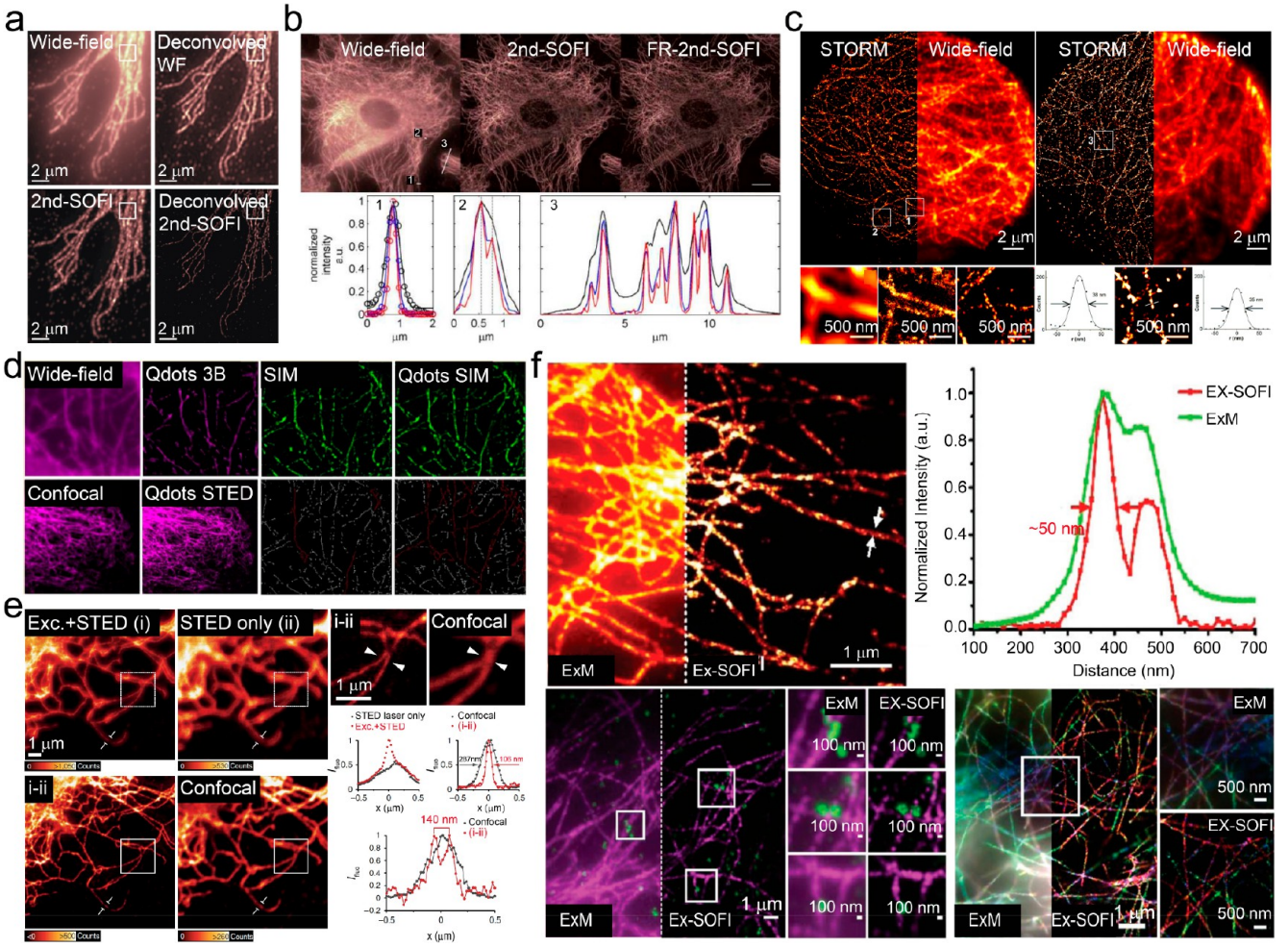

Figure 3. Qdots for super-resolution nanoscopy. (a) Wide-field and SOFI images of Qdots 625 labeled 3T3 cells. Adapted with permission from ref 58, Copyright 2009, National Academy of Sciences. (b) Wide-field and differently ordered SOFI images of Qdots 800 labeled tubulin network of 3T3 cells and corresponding line-scan intensity profiles of three regions in wide-field and SOFI nanoscopy. Adapted with permission from ref 109, Copyright 2010, Optical Society of America. (c) STORM and wide-field images of Qdots 565 and Qdots 705 labeled microtubules in HepG2 cells and profiles of specific regions in upper panel. Adapted with permission from ref 115, Copyright 2015, American Chemical Society. (d) STED, ThreeB, and SIM nanoscopy images of Qdots labeled microtubules in HeLa cells. Adapted with permission from ref 116, Copyright 2016, American Chemical Society. (e) STED images with different excitation conditions and confocal images of Qdots 705 labeled vimentin fibers. Line profiles indicated by white lines and arrows. Adapted with permission from ref 117, Copyright 2015, Nature Publishing Group. (f) ExM and ExSOFI images of Qdots 655 labeled microtubules and line-profiles indicated by white arrows. Dual-color ExM and Ex-SOFI images of Qdots 605 labeled clathrin-coated pits and Qdots 655 labeled microtubules. Multicolor ExM and Ex-SOFI images of Qdots 605 labeled acetylated microtubule, Qdots 655 labeled tyrosinated microtubule, and Qdots 705 labeled detyrosinated microtubules. Adapted with permission from ref 73, Copyright 2018, The Royal Society of Chemistry.

al. reported a series of pH-dependent photoswitchable rhodamine-based fluorescent probes with inherent blinking and applied them in STORM nanoscopy to achieve ~70 nm spatial resolution.[95] Besides the rhodamine and its derivates, Xanthene, cyanine dyes, BODIPY based and commercial dyes are also widely used in SMLM nanoscopy.[96−100]

The SMLM nanoscopy improved spatial resolution by sacrificing the temporal resolution, whereas SOFI nanoscopy that based on fluctuation property of fluorescent probes has a balanced spatial−temporal resolution. The commercial Alexa dyes are widely used in SOFI nanoscopy. In 2010, Weiss et al. introduced Alexa 647 into SOFI nanoscopy for the first time.[101] As shown in Figure 2d, after SOFI reconstruction, about 169 nm spatial resolution of Alexa 647 immunolabeled β-tubulin network in COS-7 cells was obtained.[101] Leutenegger et al. introduced a multiplexed imaging scheme to obtain 3D-SOFI images simultaneously rather than sequential imaging of multiple depth positions.[57,102] 3D-SOFI images encoded by z-axial depth of Alexa 647 stained mitochondria in fixed C2C12 cells shown in Figure 2e indicated the lateral resolution and axial resolution are 110 and 500 nm, respectively.[103] Lasser et al. used Alexa 647 dye to label microtubules in HeLa cells, mouse hippocampal primary neurons, and RAW macrophage in multiplane phase retrieval combined 3D-balanced SOFI (Figure 2f).[104]

Modified DNA probes with chemical fluorophores was originally used for Expansion Microscopy. Boyden et al. use gel-linkable DNA labels bearing Alexa 488, Atto 565, or Atto 647N to achieve nanoscale ExM imaging (~70 nm) of thick brain tissues on diffraction-limited microscope.[69] Cyanine fluorophores and Alexa 647 were not recommended because they undergo strong bleaching during the polymerization process in the ExM protocol. Boyden et al. and Vaughan et al. improved the ExM method with simplified workflows that use

https://dx.doi.org/10.1021/acs.bioconjchem.0c00320
Bioconjugate Chem. 2020, 31, 1857−1872

secondary antibodies conjugated with chemical fluorophores to visualize nanoscale biomolecules in cells and mammalian tissues.[70,84] Small-molecule fluorophores extensively used in these ExM variants were Alexa Fluor (Alexa 405, Alexa 488, Alexa 546, Alexa 568) dyes and Atto dyes (Atto 488, Atto 565, Atto 647N). However, most of these organic dyes suffer acute fluorescent loss caused by physical dilution and chemical treatment, and the fluorescent retained less than 50% of their original fluorescence intensity, which may constrain the detection of low abundant biomolecules.[84] Chung et al. introduced a similar super-resolution method, called magnified analysis of the proteome (MAP), which uses more than 100 fluorescently conjugated antibodies for multiple rounds of immunolabeling of tissue's expanded proteome, demonstrating nanoscale imaging of multiscale organization of intact mouse tissues.[105]

Small molecule dyes with specialized properties were also involved in the combination of ExM with other super-resolution microscopy, including SIM and STED.[72,106−108] As SIM do not have special requirements for fluorophores, Cahoon et al. selected commonly used Alexa Fluor 488, Alexa Fluor 555, and Atto 647N secondary antibodies in the combination method of ExM and SIM, which enables visualization of the dual-layered synaptonemal complex (SC) and accurate 3D SC organization of *Drosophila*. Helge Ewers et al. used Abberior Star Red coupled secondary antibody for labeling microtubules and demonstrated a 10 nm spatial resolution in 2D and a 50 nm resolution in 3D using ExSTED super-resolution microscopy.[72] Small molecule dyes are versatile probes and widely used in fluorescent imaging. Dyes with modified structures and targeting groups can be specifically delivered to subcellular organelles. However, the resistance to photobleaching is an important factor for super-resolution imaging.

3.2. Quantum Dots (Qdots). Quantum dots are semiconductor nanoparticles with tunable emission wavelength by varying the particle diameter, which is determined by quantum confinement effect. Bare Qdots generally show irregular photoblinking under laser excitation. The photoblinking of Qdots is a drawback and should be avoided for industrial applications, such as lightning display and long-term single-particle tracking. However, the photoblinking property is suitable for SOFI nanoscopy. Enderlein et al. proposed the principle of SOFI nanoscopy and demonstrated resolution enhancement with Qdots labeled microtubule in 3T3 cells (Figure 3a).[58] Weiss et al. developed SOFI algorithm by introducing a reweighting optical transfer function method to improve the spatial resolution in SOFI reconstruction. As shown in Figure 3b, the spatial resolution of Qdots 800 labeled tubulin network in 3T3 fibroblast show about 1.98-fold enhancement in second-order SOFI as compared with conventional widefield microscopy.[109]

Compared with other photoswitchable probes, QDs spend a rather short time in the off-state, thus limiting their application in SMLM nanoscopy. An interesting technique allows for blue-shifting of the emissions of Qdots stochastically in oxygen containing solutions can address this problem and make them suitable for STORM nanoscopy. This blue shift was attributed to the reduction of CdSe core caused by photo-oxidation and the quantum confinement effect.[110−114] Based on this principle, Kner et al. optimized the blueing speed by optimizing the laser intensity and the mounting medium (20% v/v glycerol in phosphate-buffered saline) to balance the photon number and the precise localization in STORM nanoscopy. As shown in Figure 3c, they demonstrated that 38 nm spatial resolution STORM nanoscopy with blueing processed Qdots 565 and Qdots 705 labeled microtubules in HepG2 cells.[115] Xi et al. systematically investigated applications of Qdots in STED, SIM, and ThreeB nanoscopy (Figure 3d).[116] They chose a 775 nm continuous-wave depletion laser in STED nanoscopy rather than a pulsed picosecond laser to alleviate the re-excitation and two-photon excitation of Qdots 705. An 85 nm spatial resolution of Qdots 705 labeled microtubule network in HeLa cells was achieved. Furthermore, they evaluated the continuity by calculating the pixel numbers of the microtubule structures. At last, the Qdots based ThreeB nanoscopy reveal 67 nm spatial resolution in microtubule network. ThreeB nanoscopy allows multiple emitters within the focal volume when in the on-state, and this statistical blinking can be used to generate the super-resolution image. However, this technique relies heavily on computation power to process a large amount of images for reconstruction of a relatively small image data set.[116]

Hell et al. utilized commercial ZnS-coated CdSe Qdots (~650−770 nm emission band) in STED nanoscopy.[117] In their experiments, they discovered that the Qdots can be re-excited by the 775 nm pulse depletion laser (1.2 ns pulse duration), even though far away from the emission spectra tail under about 300 mW average power. By varying the temporal delay between the excitation and depletion pulses, they proved that the STED beam can directly inhibit the spontaneous radiative decay of the on-state. As shown in Figure 3e, Qdots 705 labeled cellular vimentin fibers was resolved in STED nanoscopy with a 2.7-fold improvement of spatial resolution as compared with confocal microscopy.[117] Qu et al. achieved about 21 nm resolution in STED nanoscopy with commercial CdSe@ZnS Qdots 526 using 488 nm excitation laser and a 592 nm depletion laser to alleviated the halo effect of Qdots re-excitation.[118] To satisfy the Nyquist sampling criteria, the labeling density of nanoscopy is a key factor to obtain high-quality super-resolution images, especially in ExM-correlated approaches, i.e., Ex-SOFI and Ex-STED. Sun et al. have improved subcellular labeling density and fluorescence retention in expansion enhanced nanoscopy.[73] As shown in Figure 3f, by optimizing the concentration of glutaraldehyde (0.25%) and the incubation time (30 min) of the labeling procedure, ExM nanoscopy was obtained in Qdots 655 labeled microtubules. After acquisition of 2000 frames of images of expanded samples and SOFI analysis, about 50 nm spatial resolution was obtained in Ex-SOFI nanoscopy. Moreover, they demonstrated dual-color Ex-SOFI of Qdots 605 labeled clathrin-coated pits (CCPs) and Qdots 655 labeled microtubules. Similarly, they utilized three types of Qdots (Qdots 605, Qdots 655, and Qdots705) to label different modified tubulins simultaneously and obtained multicolor Ex-SOFI nanoscopy images with better resolution and higher contrast compared with conventional ExM (Figure 3f).[73] Qdots are composed of cadmium element that show toxicity to living cells. Therefore, developing low-toxicity or nontoxic Qdots is useful for super-resolution techniques.

3.3. Carbon Dots (Cdots). In recent years, Cdots have been widely used in fluorescent ink printing and light therapy due to a simple synthesis and preparation method.[119−121] Cdots have also been applied in STED, SOFI, and STORM super-resolution fluorescence imaging. Pompa et al. prepared Cdots with polyethylene glycol (PEG) on the surface using a

https://dx.doi.org/10.1021/acs.bioconjchem.0c00320
Bioconjugate Chem. 2020, 31, 1857−1872

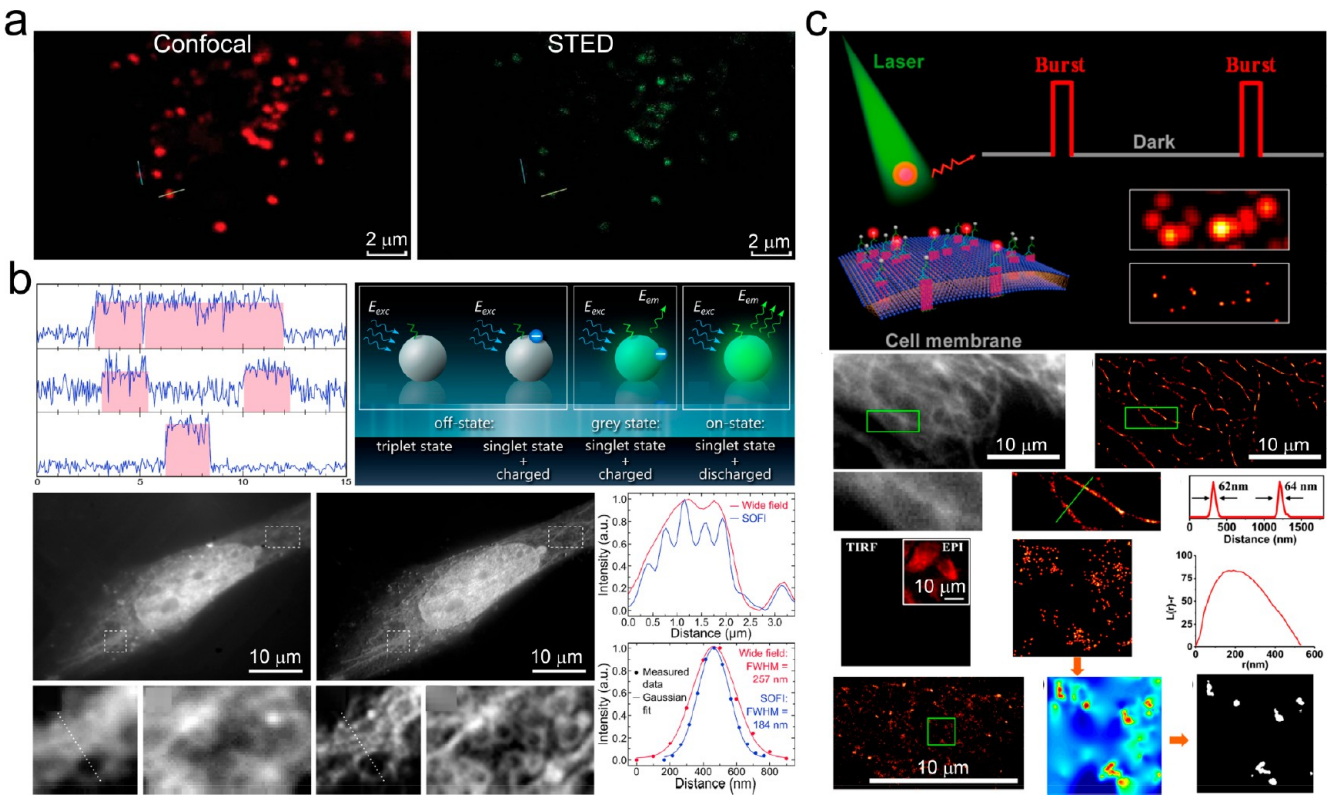

Figure 4. Cdots for super-resolution nanoscopy. (a) Confocal and STED images of Cdots in fixed MCF-7 cells. Adapted with permission from ref 122, Copyright 2014, The Royal Society of Chemistry. (b) Fluorescence time traces of individual Cdots and possible mechanism of on-, off-, and gray states of Cdots (upper-panel). Comparison of wide-field and second-order SOFI images of Cdots in Saos-2 cells and corresponding line-scan profiles. Adapted with permission from ref 123, Copyright 2016, American Chemical Society. (c) Schematic diagram of photoswitchable Cdots. Wide-field microscopy and STORM nanoscopy of Cdots labeled microtubules and cell membrane. Adapted with permission from ref 124, Copyright 2017, American Chemical Society.

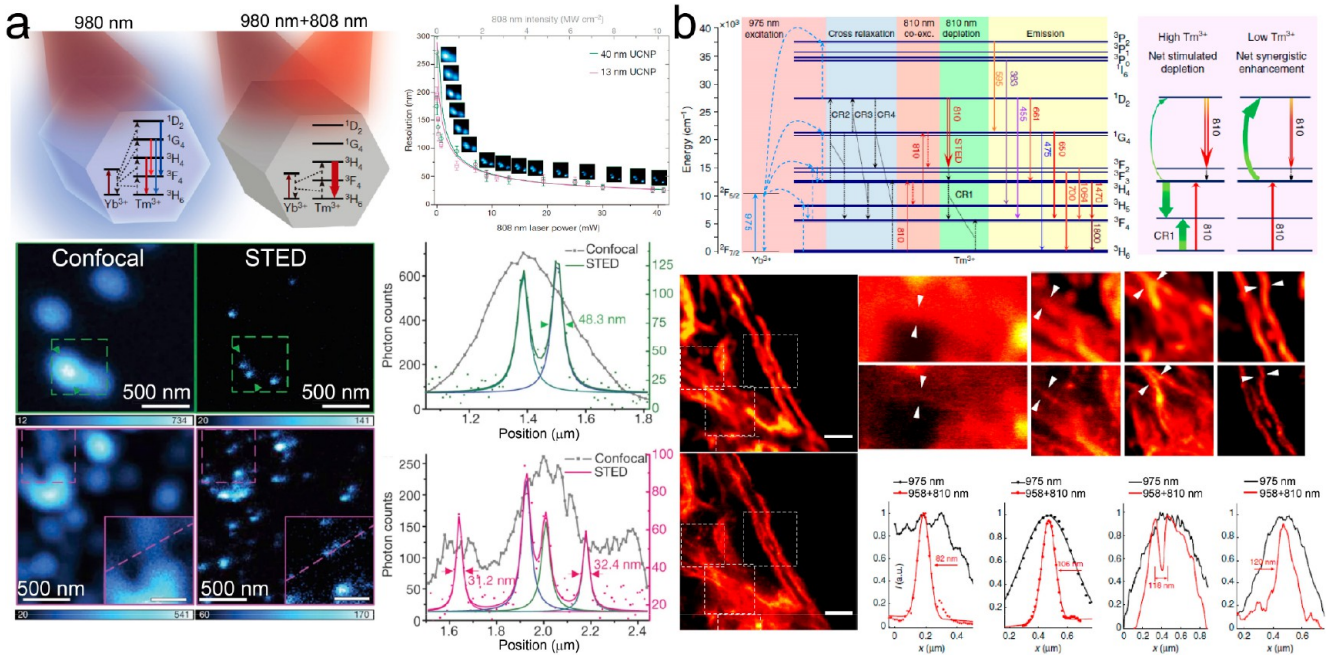

Figure 5. UCNPs for super-resolution nanoscopy. (a) Energy diagram of high concentration of Tm^{3+} doped UCNPs with two illumination schemes (left top panel). Relationship of STED resolution of single-particle UCNPs and the 808 nm depletion laser intensity (right top panel). Confocal and STED nanoscopy of 8% Tm^{3+}-doped UCNPs and corresponding line-scan profiles (lower panel). Adapted with permission from ref 132, Copyright 2017, Nature Publishing Group. (b) Optical depletion mechanism of the 455 nm upconversion luminescence in NaYF4:18% Yb^{3+}, 10% Tm^{3+}; STED nanoscopy of UCNPs labeled cytoskeleton. Adapted with permission from ref 133, Copyright 2017, Nature Publishing Group.

https://dx.doi.org/10.1021/acs.bioconjchem.0c00320
Bioconjugate Chem. 2020, 31, 1857−1872

laser ablation method.[122] Single-particle Cdots achieved a resolution of 54 nm when applied in STED. As shown in Figure 4a, after 48 h of coincubation of Cdots and MCF-7 cells, the STED images show that the best resolution obtained was 30 nm. However, Cdots were not able to label specific subcellular targets; they only showed distribution spreading in the cytoplasm, indicating that further development is needed for functional imaging for subcellular structures.[122] Chizhik et al. prepared green luminescent Cdots using citric acid and urea as carbon and nitrogen sources by hydrothermal synthesis. Single-particle fluorescence intensity of Cdots indicated that Cdots show obvious photoblinking properties. By incubating Cdots with Saos-2 cells, the super-resolved fluorescence image with a spatial resolution of 180 nm can be reconstructed by second-order SOFI analysis (Figure 4b).[123] Recently, Huang et al. prepared photoblinking Cdots by mixing carbon powder and citric acid by centrifugation. The long off-time cycle indicated the Cdots are suitable for STORM imaging. As shown in Figure 4c, they conjugated Cdots with secondary antibody IgG, which allows labeling of subcellular structures with high specificity. The STORM results showed that about a 64 nm resolution can be achieved of Cdots-labeled microtubules in HeLa cell.[124] For Cdots, the functionalization for specific subcellular labeling is still a challenge. The bioconjugation of Cdots is crucial for their applications in super-resolution imaging techniques.

3.4. Upconversion Nanoparticles (UCNPs). Most luminescent materials show down-converted emission under light excitation. A series of unique materials show opposite properties with frequency upconversion under long-wavelength excitation. The upconversion nanoparticles (UCNPs) are usually composed of lanthanide compounds and are of particular applications in bioimaging, biosensing, and nanomedicine.[125−129] Interestingly, UCNPs have also been applied in super-resolution nanoscopy.

At the nanometer scale, the phase, dimension, and doping level of lanthanide-doped UCNPs can be precisely controlled.[130,131] The inorganic crystals doped with lanthanide ions can easily establish a population inversion caused by the metastable energy level of the trivalent lanthanide ions and can produce amplified excited emission at lower pump power. Jin et al. prepared UCNPs doped with high concentration (8%) of thulium ions (Tm^{3+}) NaYF4:20%Yb^{3+}, 8%Tm^{3+}.[132] Under 980 nm laser illumination, the high-concentration doping of Tm^{3+} enhanced the interaction between Tm^{3+} and results in internal cross relaxation, indicating a rapidly increasing population in $^3H_4$ energy level, which is similar to the photon avalanche effect. This process resulted in population inversion relative to the $^3H_6$ ground energy level. At this time, under the trigger of 808 nm laser, the transition from $^3H_4$ to $^3H_6$ energy levels can easily occur under stimulated emission. Thus, by illuminating with 980 and 808 nm laser simultaneously, the up-converted blue emission of Tm^{3+} from $^1G_4$ to $^3H_6$ ground energy level was inhibited, competing with the stimulation emission of 808 nm; the energy level diagram of UCNPs is shown in Figure 5a. This phenomenon exactly meets the requirements of STED super-resolution imaging technology for fluorescent probes. They built a STED imaging platform for UCNP probes with a 980 nm laser as excitation light source surrounding with a doughnut-shaped 808 nm depletion laser. Figure 5a shows the single-particle STED nanoscopy of NaYF4:20%Yb^{3+}, 8%Tm^{3+} UCNPs, indicating about 28 nm spatial resolution.[132]

At the same time, Zhan et al. prepared a higher concentration of Tm^{3+} (10%) doped in $NaYF_4$:18%Yb^{3+} UCNPs and obtained about 66 nm spatial resolution single-particle STED nanoscopy.[133] They also demonstrated dual-color UCNPs based STED nanoscopy by introducing $NaGdF_4$:40%Yb^{3+}, 10% Tm^{3+}@$NaGdF_4$:15% Tb^{3+} core−shell structures. With the catalysis of *N*-(3-(dimethylamino)propyl)-*N*′-ethylcarbodiimide hydrochloride (EDC), they prepared carboxyl functionalized UCNPs and conjugated with antibodies. As shown in Figure 5b, they labeled microtubules of HeLa cells, and about 82 nm spatial resolution was obtained in STED nanoscopy with functionalized UCNPs.[133] Jin et al. demonstrated a UCNPs based near-infrared emission saturation (NIRES) nanoscopy for deep tissue super-resolution by using a 980 nm doughnut laser beam and detecting at 800 nm. In liver tissue slices, about 50 nm resolution of single UCNPs was achieved.[134] Ågren et al. modified the emission intensity of UCNPs by adopting a high-sensitizer (Yb^{3+}) doping strategy. The strategy of enhanced emission intensity and accelerated emission kinetics of UCNPs and a spatial resolution of 72 nm was readily achieved.[135] The main restriction of UCNPs applied in super-resolution nanoscopy is the specific subcellular labeling and biocompatibility. Both of these drawbacks may be solved with new strategies, such as surface chemistry and bioconjugation methods.

3.5. Aggregation Induced Emission (AIE) Nanoparticles. Aggregation-induced emission luminogens (AIEgens) are a class of organic molecules that show luminescence in the aggregate state. This is opposite to the conventional aggregation caused quenching (ACQ) dyes and was first discovered by Tang et al. in 2001.[136] The AIE phenomenon is usually considered to be two restriction mechanisms: restriction of intramolecular rotation (RIR) and restriction of intramolecular vibration (RIV).[137,138] Because of the unique luminescence properties, AIEgen have great potential in biomedical fluorescence applications. Tang et al. developed a tetraphenylethylene (TPE) derivative named o-TPE-ON+, which is an oxygen-promoted photoactivation AIE bioprobe. Spontaneous blinking without any additives and specificity to mitochondria via membrane potential indicate that o-TPE-ON + is suitable for SMLM in live and fixed cells. They obtained about 104 nm spatial resolution of mitochondria in fixed HeLa cell and monitored the dynamic process of mitochondria in nanoscale in living cell using STORM nanoscopy.[139] Tang et al. also prepared colloidal mesoporous silica loaded 2,3-bis(4-(phenyl(4-(1,2,2-triphenylvinyl)phenyl)amino)phenyl) fumaronitrile (TTF) AIE nanoparticles incubated with HeLa cells and applied in STED nanoscopy. Benefiting from high resistance to photobleaching and high STED efficiency (more than 60%), they obtained about 30 nm lateral spatial resolution.[140] Qian et al. developed a type of mitochondria target AIEgens with higher STED efficiency (about 80%) and observed the dynamic motion, fusion, and fission of mitochondria with about 92 nm resolution under STED nanoscopy.[141] We synthesized a series of oxetane-substituted AIEgens (AIE-OXE) and developed a general approach for preparing small and bioconjugated AIE nanoparticles for specific labeling of cellular targets. We labeled microtubules in fixed cells and obtained continuous subcellular STED nanoscopy with 95 nm spatial resolution.[142]

3.6. Polymer Dots (Pdots). Polymer dots (Pdots) consisting of highly fluorescent conjugated polymers have attracted considerable interest in recent years.[143−150] Con-

https://dx.doi.org/10.1021/acs.bioconjchem.0c00320
Bioconjugate Chem. 2020, 31, 1857−1872

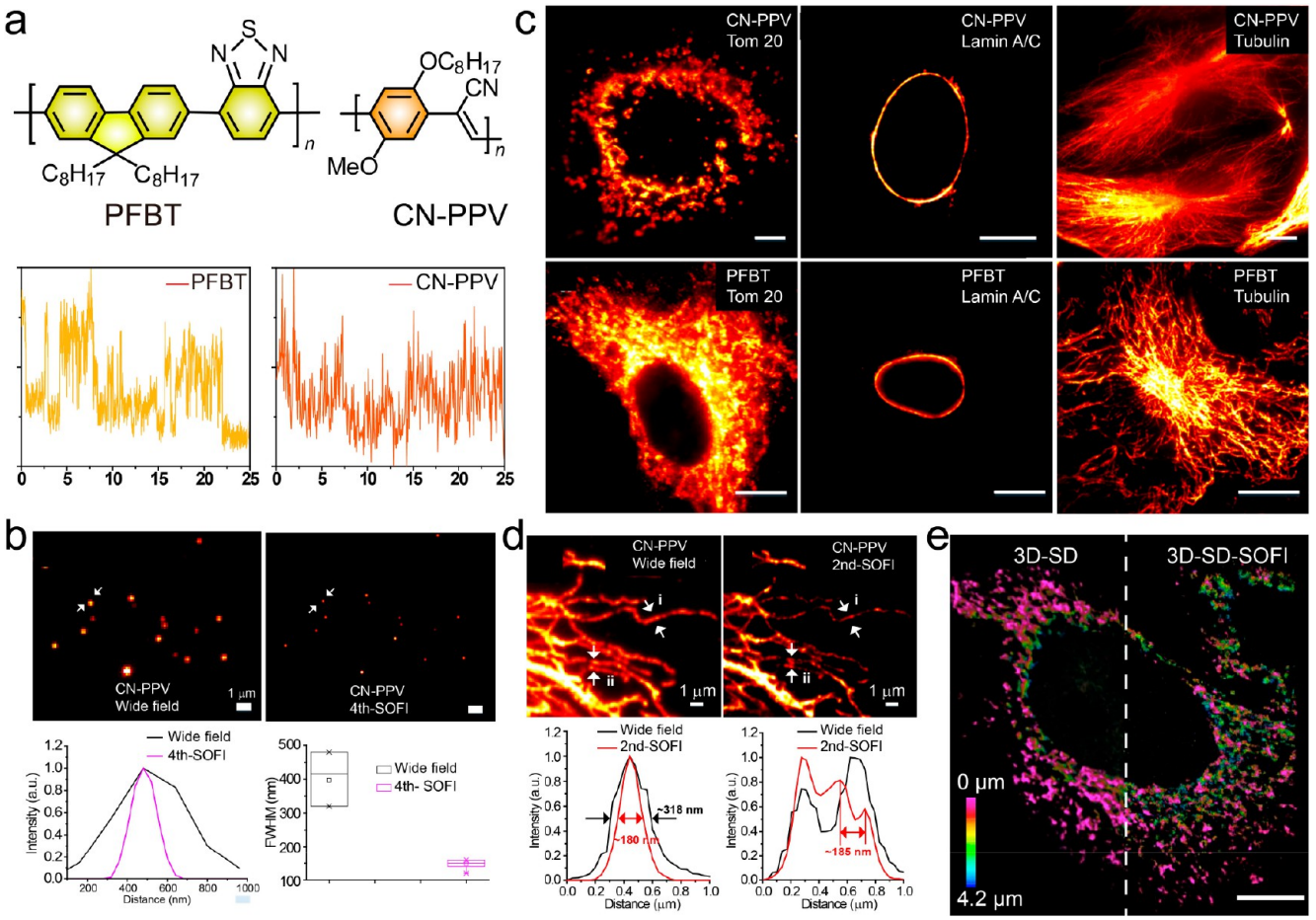

Figure 6. Small photoblinking Pdots for SOFI nanoscopy. (a) Chemical structures and single-particle photoblinking of PFBT and CN-PPV Pdots. (b) Single-particle SOFI nanoscopy of CN-PPV and corresponding spatial resolution. (c) Subcellular specific labeling images of PFBT and CN-PPV Pdots. (d) Wide-field microscopy and SOFI nanoscopy images of CN-PPV labeled microtubules in BS-C-1 cells. (e) Three-dimensional SOFI of CN-PPV Pdots labeled mitochondria membrane in BS-C-1 cell. Scale bar: 1, 10, and 10 μm for (b), (c), and (e), respectively. Adapted with permission from ref 169, Copyright 2017, John Wiley and Sons.

jugated polymers are widely used in luminescent devices, solar cells, field effect transistors, and other optoelectronic devices. Pdots can be conveniently prepared by a nanoreprecipitation method, and the size of Pdots can be modified by varying preparation conditions.[151−154] Pdots with spectrum ranging from the visible region to the near-infrared region have been widely used in fluorescence imaging, optical sensors, photoacoustic imaging, and phototherapy applications.[155−163]

The excellent photophysical properties, such as high fluorescence brightness, fast fluorescence radiation rate, and great photostability, make Pdots promising probes for supersolution imaging. The bright fluorescence of Pdots yielded a lateral particle tracking uncertainty of 1−2 nm, as determined from analysis of trajectories of fixed and freely diffusing particles.[164] There is evidence that the fluorescence of Pdots can be quenched by hole polaron, resulting in a dark spot in single particle fluorescence.[165,166] McNeill et al. have investigated the polaron motion inside Pdots with an unprecedented level of detail about charge transport. The fluorescence centroid was displaced, accompanied by the movement of dark spots, while the polaron migrated inside the particles.[167] Combined with mean square displacement (MSD) of centroid displacement, they discovered that the single-particle fluorescence is very sensitive to polaron generation and recombination dynamics. The polaron dynamics provide a promising strategy for development of photoswitching probes for localization based fluorescence nanoscopy.[168]

We have made efforts to apply Pdots in super-resolution nanoscopy by optimizing the photophysical property. In 2016, we prepared two types of photoblinking Pdots (PFBT and CN-PPV) by regulating size distributions (Figure 6a). By single-particle SOFI reconstruction of 1000 frames of raw data, we demonstrated Pdots based SOFI nanoscopy for the first time. As shown in Figure 6b, after fourth-order SOFI reconstruction, the spatial resolution of single-particle CN-PPV Pdots increased about 2.7-fold as compared with conventional wide-field microscopy. We realized specific subcellular labeling with biofunctionalized Pdots. We labeled mitochondria membrane, nuclear pore, and microtubule in BS-C-1 cells with streptavidin conjugated PFBT and CN-PPV Pdots (Figure 6c). We achieved 185 nm spatial resolution of CN-PPV labeled α-tubulin with second-order SOFI reconstruction, indicating about 1.8-fold resolution enhancement as compare with wide-field microscopy (Figure 6d). As shown in Figure 6e, three-dimensional SOFI images of CN-PPV Pdots labeled mitochondrial membrane of BS-C-1 cells was achieved by using a spinning disk confocal microscope with rapid fluorescence imaging capability.[169]

By choosing different polymer species, blue emission PFO and red emission PFTBT5 Pdots were obtained. Both PFO

https://dx.doi.org/10.1021/acs.bioconjchem.0c00320
Bioconjugate Chem. 2020, 31, 1857−1872

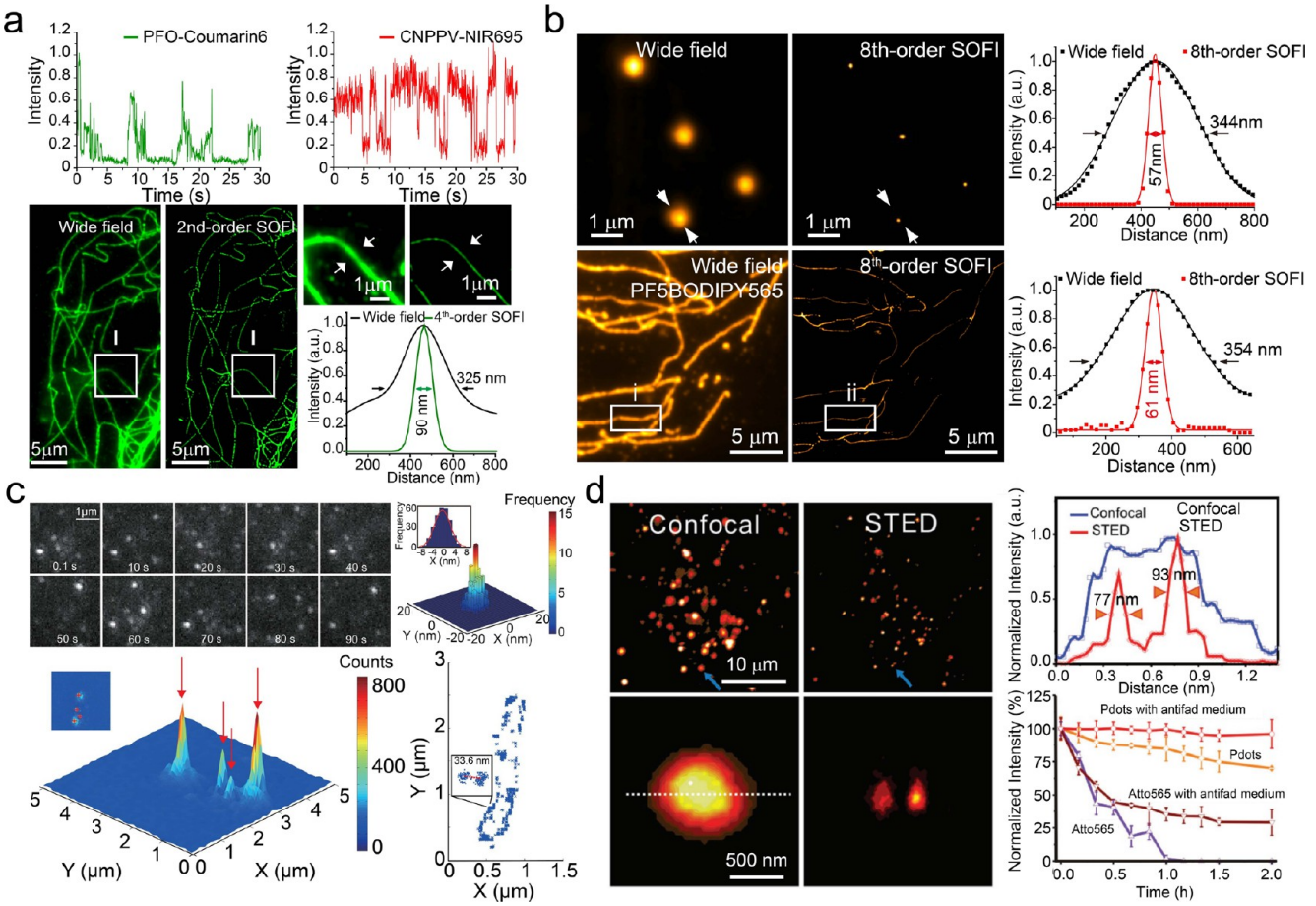

Figure 7. Pdots for super-resolution nanoscopy. (a) Photoblinking traces of cooperative blinking Pdots; fourth-order SOFI images of PFO-Coumarin6 Pdots labeled microtubules in BS-C-1 cells and line-scan profiles. Adapted with permission from ref 171, Copyright 2019, American Chemical Society. (b) Eighth-order SOFI nanoscopy of single-particle and microtubule labeled with PF5BODIPY565 Pdots. Adapted with permission from ref 173, Copyright 2020, The Royal Society of Chemistry. (c) A sequence of fluorescence microscopy images showing blinking behavior of 20% PCBM-doped PFBT Pdots and the three-dimensional histogram of localized centroid position extracted from one blinking 20% PCBM-PFBT Pdot; Three-dimensional fluorescence intensity map of switched "on" Pdots in *E. coli* and scatter plot of super-resolution image reconstructed from the localized positions of blinking Pdots. Adapted with permission from ref 168, Copyright 2019, American Chemical Society. (d) Long-term STED bioimaging of PDFDP Pdots in HeLa cells. Adapted with permission from ref 175, Copyright 2018, John Wiley and Sons.

and PFTBT5 show obvious photoblinking property. We demonstrated dual-color subcellular labeling with PFO and PFTBT5 Pdots in BS-C-1 cells simultaneously. With second-order SOFI reconstruction of PFTBT5 Pdots labeled CCPs in BS-C-1 cells, about 1.9-fold spatial resolution enhancement was seen. The hollow structure of mature CCPs was resolved with enhanced spatial resolution and signal-to-background ratio. We demonstrated dual-color SOFI nanoscopy of PFO labeled CCPs and PFTBT5 labeled microtubules. Based on intensity profile statistics, an approximate 1.67-fold enhancement of spatial resolution was obtained, and finer structures were resolved.[170]

To further improve the resolution of Pdots based SOFI nanoscopy, we prepared fluorescent dye-doped Pdots with a cooperative blinking process from the dye ensemble inside the Pdots. As shown in Figure 7a, with fourth-order SOFI analysis, we achieved 68 and 90 nm spatial resolution of single-particle and microtubule labeled with cooperative blinking Pdots, indicating about 5.3- and 3.6-fold enhancement as compared with wide-field microscopy.[171] The on/off photoblinking characteristics are key factors for realizing high-order SOFI. We introduced a strategy to modulate the photoblinking property by synthesizing multichromophoric system consisting of donor−acceptor conjugated polymers. A 98 nm spatial resolution was obtained for microtubules labeled with high-performance photoblinking Pdots.[172] With sufficient brightness and fluctuations, a higher order of image processing affords a higher resolution, and in principle, the resolution enhancement is unbounded. As shown in Figure 7b, we synthesized two types of BODIPY-based polymer dots (Pdots) with narrow-band emissions, pronounced fluctuations, and prominent photostability. A spatial resolution (61 nm) was obtained for single microtubules labeled by the BODIPY Pdots. Furthermore, we obtained 92 nm resolution in dual-color SOFI images of PF5BODIPY labeled tyrosinated microtubules and PF8BODIPY720 labeled mitochondria membrane in BS-C-1 cell.[173]

Pdots has also been explored for STORM applications. McNeill and coworkers showed that a fullerene derivative PCBM can be doped into PFBT Pdots to establish a fluctuating steady-state population of tens of hole polarons, which can sufficiently suppress the fluorescence of the Pdots. However, burst emissions can be released from the PCBM doped Pdots owing to the fluctuations in the number of charge carriers. As shown in Figure 7c, they used the PCBM doped Pdots in STORM nanoscopy and 576 obtained about 33.6 nm

https://dx.doi.org/10.1021/acs.bioconjchem.0c00320
Bioconjugate Chem. 2020, 31, 1857−1872

spatial resolution with a localization precision of ~0.6 nm.[168] In a latest study, McNeill et al. employed the doping strategy to modulate the hole-polarons inside the Pdots, thus regulating the spontaneous switching and photoswitching properties to operate in two super-resolution imaging modes. By optimizing the doping ratio and illumination scheme of photoactive laser to regulating the "ON" state duty cycle, they obtained spontaneous switching and photoswitching enabled STORM nanoscopy. They demonstrated 3D-STORM imaging of microtubules and CCPs with about 45 nm spatial resolution in fixed BS-C-1 cells. The ring-shaped structure of CCPs in dual-color STORM images can be observed, which is consistent with the hollow spherical structure of CCPs.[174]

Besides the SOFI and STORM application of Pdots, Fang et al. prepared PDFDP Pdots and applied in STED nanoscopy, indicating that Pdots are a new class of fluorescent probe for STED nanoscopy. The PDFDP Pdots show about 77 nm spatial resolution in STED image and excellent photostability in STED nanoscopy incubated with fixed HeLa cells.[175] Pdots with high emission brightness, high quantum yield efficiency, and biocompatibility are a type of emerging fluorescent probes with versatile conjugation ability. With sufficient developing and new strategies to manipulate the photophysical properties, Pdots will show a wide range of applications in fluorescent nanoscopy.

4. CONCLUSIONS AND PERSPECTIVES

The development of super-resolution fluorescence imaging techniques is of great significance and provides a great deal of detail in various studies in cell biology and biomedicine. The performance of these imaging techniques is largely dependent on the photophysical properties of the fluorescent probes. Because the working principles of the super-resolution techniques are different, each imaging modality has specific requirements for the fluorescent probes in terms of their photophysical parameters. Until now, a large number of fluorescent probes have been developed for super-resolution nanoscopy, resulting in visualization of subcellular spatial organization, molecular interaction, molecular counting, and temporal dynamics under unprecedented resolutions. Despite the versatile progress, each of the fluorescent probes has its own advantages and shortcomings and should be tailored in case-specific studies as follows: (i) Fluorescent proteins and organic dyes are mature and the most widely used probes in supersolution imaging, but they suffer from poor photostability and low brightness, which restricted long-term tracking in living cells for monitoring the dynamic processes and the interactions between different subcellular organelles. (ii) The exogenous nanoparticle probes showed improved brightness and photostability, which are advantageous for long-term cell imaging. However, high-quality specific subcellular labeling remains a challenge for the nanoparticle labels because the complex interactions of nanoparticles with cellular structures often results in intractable nonspecific binding. In addition, conjugation of specific biomolecules to the nanoparticles also encounters issues such as cross-linking, aggregation, and colloidal stability, as each nanoparticle often has multiple reactive groups. A common issue for those exogenous nanoparticles is the difficulty in live-cell imaging. Development of cell-permeable probes or utilizing peptide vehicle may help to deliver nanoparticles into living cells. (iii) So far, application of super-resolution for *in vivo* and clinical samples with large imaging field and deep imaging depth are still big challenges. In optical imaging techniques, the spatial resolution and the imaging depth are mutually restricted factors. Therefore, developing an imaging system with super-resolution, large field of view, and imaging depth is a key problem to be solved. (iv) Finally, it is worth mentioning that most of the super-resolution techniques, such as STED, SIM, and STORM, rely on complicated imaging setups, while SOFI and ExM rely exclusively on fluorescent probes and the biological sample. ExM has been developed rapidly by virtue of sample expansion and imaging on commercial confocal microscope. Combination of ExM with STED, STORM, and SOFI may be a promising solution to further improve the spatial resolution in imaging of biological tissues. In all cases, a common requirement to improve the imaging quality is that the probe conjugates should emit bright signals and exhibit specific labeling with minimal nonspecific binding in subcellular environment.

AUTHOR INFORMATION

Corresponding Author

Changfeng Wu − *Department of Biomedical Engineering, Southern University of Science and Technology, Shenzhen, Guangdong 510855, China;* orcid.org/0000-0001-6797-9784; Email: wucf@sustech.edu.cn

Authors

Zhihe Liu − *Department of Biomedical Engineering, Southern University of Science and Technology, Shenzhen, Guangdong 510855, China;* orcid.org/0000-0002-5134-4116

Jie Liu − *Department of Biomedical Engineering, Southern University of Science and Technology, Shenzhen, Guangdong 510855, China; Department of Biology, Hong Kong Baptist University, Hong Kong 999077, China*

Xiaodong Wang − *Department of Biomedical Engineering, Southern University of Science and Technology, Shenzhen, Guangdong 510855, China*

Feixue Mi − *Department of Biomedical Engineering, Southern University of Science and Technology, Shenzhen, Guangdong 510855, China*

Dan Wang − *Key Laboratory of Functional Inorganic Material Chemistry, Ministry of Education, School of Chemistry and Materials Science, Heilongjiang University, Harbin 150080, China*

Complete contact information is available at: https://pubs.acs.org/10.1021/acs.bioconjchem.0c00320

Notes

The authors declare no competing financial interest.

ACKNOWLEDGMENTS

C. Wu acknowledges financial support by the grants from Shenzhen Science and Technology Innovation Commission (Grant No. KQTD20170810111314625) and the National Natural Science Foundation of China (Grant No. 81771930).

REFERENCES

(1) Liu, T. L., Upadhyayula, S., Milkie, D. E., Singh, V., Wang, K., Swinburne, I. A., Mosaliganti, K. R., Collins, Z. M., Hiscock, T. W., Shea, J., et al. (2018) Observing the cell in its native state: Imaging subcellular dynamics in multicellular organisms. *Science 360*, eaaq1392.

(2) Sigal, Y. M., Zhou, R., and Zhuang, X. (2018) Visualizing and discovering cellular structures with super-resolution microscopy. *Science 361*, 880−887.
(3) Guo, Y., Li, D., Zhang, S., Yang, Y., Liu, J. J., Wang, X., Liu, C., Milkie, D. E., Moore, R. P., Tulu, U. S., et al. (2018) Visualizing Intracellular Organelle and Cytoskeletal Interactions at Nanoscale Resolution on Millisecond Timescales. *Cell 175*, 1430−1442.
(4) York, A. G., Chandris, P., Dalle Nogare, D., Head, J., Wawrzusin, P., Fischer, R. S., Chitnis, A., and Shroff, H. (2013) Instant super-resolution imaging in live cells and embryos via analog image processing. *Nat. Methods 10*, 1122−1126.
(5) Grimm, J. B., English, B. P., Chen, J., Slaughter, J. P., Zhang, Z., Revyakin, A., Patel, R., Macklin, J. J., Normanno, D., and Singer, R. H. (2015) A general method to improve fluorophores for live-cell and single-molecule microscopy. *Nat. Methods 12*, 244−250.
(6) Chu, L. A., Lu, C. H., Yang, S. M., Liu, Y. T., Feng, K. L., Tsai, Y. C., Chang, W. K., Wang, W. C., Chang, S. W., Chen, P., et al. (2019) Rapid single-wavelength lightsheet localization microscopy for clarified tissue. *Nat. Commun. 10*, 1−10.
(7) Ahrens, M. B., Orger, M. B., Robson, D. N., Li, J. M., and Keller, P. J. (2013) Whole-brain functional imaging at cellular resolution using light-sheet microscopy. *Nat. Methods 10*, 413−420.
(8) Neef, J., Urban, N. T., Ohn, T. L., Frank, T., Jean, P., Hell, S. W., Willig, K. I., and Moser, T. (2018) Quantitative optical nanophysiology of $Ca2^{+}$ signaling at inner hair cell active zones. *Nat. Commun. 9*, 1−17.
(9) Pennacchietti, F., Serebrovskaya, E. O., Faro, A. R., Shemyakina, I. I., Bozhanova, N. G., Kotlobay, A. A., Gurskaya, N. G., Bodén, A., Dreier, J., Chudakov, D. M., et al. (2018) Fast reversibly photoswitching red fluorescent proteins for live-cell RESOLFT nanoscopy. *Nat. Methods 15*, 601−604.
(10) Gwosch, K. C., Pape, J. K., Balzarotti, F., Hoess, P., Ellenberg, J., Ries, J., and Hell, S. W. (2020) MINFLUX nanoscopy delivers 3D multicolor nanometer resolution in cells. *Nat. Methods 17*, 217−224.
(11) Culley, S., Albrecht, D., Jacobs, C., Pereira, P. M., Leterrier, C., Mercer, J., and Henriques, R. (2018) Quantitative mapping and minimization of super-resolution optical imaging artifacts. *Nat. Methods 15*, 263−266.
(12) Wang, C., Taki, M., Sato, Y., Fukazawa, A., Higashiyama, T., and Yamaguchi, S. (2017) Super-Photostable Phosphole-Based Dye for Multiple-Acquisition Stimulated Emission Depletion Imaging. *J. Am. Chem. Soc. 139*, 10374−10381.
(13) Gottfert, F., Pleiner, T., Heine, J., Westphal, V., Gorlich, D., Sahl, S. J., and Hell, S. W. (2017) Strong signal increase in STED fluorescence microscopy by imaging regions of subdiffraction extent. *Proc. Natl. Acad. Sci. U. S. A. 114*, 2125−2130.
(14) Balzarotti, F., Eilers, Y., Gwosch, K. C., Gynnå, A. H., Westphal, V., Stefani, F. D., Elf, J., and Hell, S. W. (2017) Nanometer resolution imaging and tracking of fluorescent molecules with minimal photon fluxes. *Science 355*, 606−612.
(15) Grotjohann, T., Testa, I., Leutenegger, M., Bock, H., Urban, N. T., Lavoie-Cardinal, F., Willig, K. I., Eggeling, C., Jakobs, S., and Hell, S. W. (2011) Diffraction-unlimited all-optical imaging and writing with a photochromic GFP. *Nature 478*, 204−208.
(16) Hell, S. W. (2007) Far-Field Optical Nanoscopy. *Science 316*, 1153−1158.
(17) Willig, K. I., Kellner, R. R., Medda, R., Hein, B., Jakobs, S., and Hell, S. W. (2006) Nanoscale resolution in GFP-based microscopy. *Nat. Methods 3*, 721−723.
(18) Klar, T. A., Jakobs, S., Dyba, M., Egner, A., and Hell, S. W. (2000) Fluorescence microscopy with diffraction resolution barrier broken by stimulated emission. *Proc. Natl. Acad. Sci. U. S. A. 97*, 8206−8210.
(19) Hell, S. W., and Wichmann, J. (1994) Breaking the diffraction resolution limit by stimulated emission: stimulated-emission-depletion fluorescence microscopy. *Opt. Lett. 19*, 780−782.
(20) Turcotte, R., Liang, Y., Tanimoto, M., Zhang, Q., Li, Z., Koyama, M., Betzig, E., and Ji, N. (2019) Dynamic super-resolution structured illumination imaging in the living brain. *Proc. Natl. Acad. Sci. U. S. A. 116*, 9586−9591.
(21) Zhang, X., Zhang, M., Li, D., He, W., Peng, J., Betzig, E., and Xu, P. (2016) Highly photostable, reversibly photoswitchable fluorescent protein with high contrast ratio for live-cell super-resolution microscopy. *Proc. Natl. Acad. Sci. U. S. A. 113*, 10364−10369.
(22) Li, D., Shao, L., Chen, B. C., Zhang, X., Zhang, M., Moses, B., Milkie, D. E., Beach, J. R., Hammer, J. A., Pasham, M., et al. (2015) Extended-resolution structured illumination imaging of endocytic and cytoskeletal dynamics. *Science 349*, aab3500.
(23) Rego, E. H., Shao, L., Macklin, J. J., Winoto, L., Johansson, G. A., Kamps-Hughes, N., Davidson, M. W., and Gustafsson, M. G. (2012) Nonlinear structured-illumination microscopy with a photoswitchable protein reveals cellular structures at 50-nm resolution. *Proc. Natl. Acad. Sci. U. S. A. 109*, 135−143.
(24) Gustafsson, M. G. L. (2005) Nonlinear structured-illumination microscopy: Wide-field fluorescence imaging with theoretically unlimited resolution. *Proc. Natl. Acad. Sci. U. S. A. 102*, 13081−13086.
(25) Gustafsson, M. G. L. (2000) Surpassing the lateral resolution limit by a factor of two using structured illumination microscopy. *J. Microsc. 198*, 82−87.
(26) Oracz, J., Adolfsson, K., Westphal, V., Radzewicz, C., Borgstrom, M. T., Sahl, S. J., Prinz, C. N., and Hell, S. W. (2017) Ground State Depletion Nanoscopy Resolves Semiconductor Nanowire Barcode Segments at Room Temperature. *Nano Lett. 17*, 2652−2659.
(27) Folling, J., Bossi, M., Bock, H., Medda, R., Wurm, C. A., Hein, B., Jakobs, S., Eggeling, C., and Hell, S. W. (2008) Fluorescence nanoscopy by ground-state depletion and single-molecule return. *Nat. Methods 5*, 943−945.
(28) Hell, S. W., and Kroug, M. (1995) Ground-state-depletion fluorscence microscopy A concept for breaking the diffraction resolution limit. *Appl. Phys. B: Lasers Opt. 60*, 495−497.
(29) Wang, S., Chen, X., Chang, L., Xue, R., Duan, H., and Sun, Y. (2016) GMars-Q Enables Long-Term Live-Cell Parallelized Reversible Saturable Optical Fluorescence Transitions Nanoscopy. *ACS Nano 10*, 9136−9144.
(30) Bohm, U., Hell, S. W., and Schmidt, R. (2016) 4Pi-RESOLFT nanoscopy. *Nat. Commun. 7*, 1−8.
(31) Tiwari, D. K., Arai, Y., Yamanaka, M., Matsuda, T., Agetsuma, M., Nakano, M., Fujita, K., and Nagai, T. (2015) A fast- and positively photoswitchable fluorescent protein for ultralow-laser-power RESOLFT nanoscopy. *Nat. Methods 12*, 515−518.
(32) Testa, I., D'Este, E., Urban, N. T., Balzarotti, F., and Hell, S. W. (2015) Dual channel RESOLFT nanoscopy by using fluorescent state kinetics. *Nano Lett. 15*, 103−106.
(33) Hofmann, M., Eggeling, C., Jakobs, S., and Hell, S. W. (2005) Breaking the diffraction barrier in fluorescence microscopy at low light intensities by using reversibly photoswitchable proteins. *Proc. Natl. Acad. Sci. U. S. A. 102*, 17565−17569.
(34) Roubinet, B., Bossi, M. L., Alt, P., Leutenegger, M., Shojaei, H., Schnorrenberg, S., Nizamov, S., Irie, M., Belov, V. N., and Hell, S. W. (2016) Carboxylated Photoswitchable Diarylethenes for Biolabeling and Super-Resolution RESOLFT Microscopy. *Angew. Chem., Int. Ed. 55*, 15429−15433.
(35) Rust, M. J., Bates, M., and Zhuang, X. (2006) Sub-diffraction-limit imaging by stochastic optical reconstruction microscopy (STORM). *Nat. Methods 3*, 793−795.
(36) Bates, M., Huang, B., Dempsey, G. T., and Zhuang, X. (2007) Multicolor Super-Resolution Imaging with Photo-Switchable Fluorescent Probes. *Science 317*, 1749−1753.
(37) Huang, B., Wang, W., Bates, M., and Zhuang, X. (2008) Three-Dimensional Super-Resolution Imaging by Stochastic Optical Reconstruction Microscopy. *Science 319*, 810−813.
(38) Huang, B., Bates, M., and Zhuang, X. (2009) Super-resolution fluorescence microscopy. *Annu. Rev. Biochem. 78*, 993−1016.

https://dx.doi.org/10.1021/acs.bioconjchem.0c00320
Bioconjugate Chem. 2020, 31, 1857−1872

(39) Jones, S. A., Shim, S. H., He, J., and Zhuang, X. (2011) Fast, three-dimensional super-resolution imaging of live cells. *Nat. Methods 8*, 499−508.
(40) Xu, K., Babcock, H. P., and Zhuang, X. (2012) Dual-objective STORM reveals three-dimensional filament organization in the actin cytoskeleton. *Nat. Methods 9*, 185−188.
(41) Mukamel, E. A., Babcock, H., and Zhuang, X. (2012) Statistical deconvolution for superresolution fluorescence microscopy. *Biophys. J. 102*, 2391−2400.
(42) Dempsey, G. T., Vaughan, J. C., Chen, K. H., Bates, M., and Zhuang, X. (2011) Evaluation of fluorophores for optimal performance in localization-based super-resolution imaging. *Nat. Methods 8*, 1027−1036.
(43) Jia, S., Vaughan, J. C., and Zhuang, X. (2014) Isotropic 3D Super-resolution Imaging with a Self-bending Point Spread Function. *Nat. Photonics 8*, 302−306.
(44) Boettiger, A. N., Bintu, B., Moffitt, J. R., Wang, S., Beliveau, B. J., Fudenberg, G., Imakaev, M., Mirny, L. A., Wu, C. T., and Zhuang, X. (2016) Super-resolution imaging reveals distinct chromatin folding for different epigenetic states. *Nature 529*, 418−422.
(45) Bintu, B., Mateo, L. J., Su, J. H., Sinnott-Armstrong, N. A., Parker, M., Kinrot, S., Yamaya, K., Boettiger, A. N., and Zhuang, X. (2018) Super-resolution chromatin tracing reveals domains and cooperative interactions in single cells. *Science 362*, eaau1783.
(46) Betzig, E., Patterson, G. H., Sougrat, R., Lindwasser, O. W., Olenych, S., Bonifacino, J. S., Davidson, M. W., Lippincott-Schwartz, J., and Hess, H. F. (2006) Imaging intracellular fluorescent proteins at nanometer resolution. *Science 313*, 1642−1645.
(47) Shroff, H., Galbraith, C. G., Galbraith, J. A., White, H., Gillette, J., Olenych, S., Davidson, M. W., and Betzig, E. (2007) Dual-color superresolution imaging of genetically expressed probes within individual adhesion complexes. *Proc. Natl. Acad. Sci. U. S. A. 104*, 20308−20313.
(48) Manley, S., Gillette, J. M., Patterson, G. H., Shroff, H., Hess, H. F., Betzig, E., and Lippincott-Schwartz, J. (2008) High-density mapping of single-molecule trajectories with photoactivated localization microscopy. *Nat. Methods 5*, 155−157.
(49) Shroff, H., Galbraith, C. G., Galbraith, J. A., and Betzig, E. (2008) Live-cell photoactivated localization microscopy of nanoscale adhesion dynamics. *Nat. Methods 5*, 417−423.
(50) Shtengel, G., Galbraith, J. A., Galbraith, C. G., Lippincott-Schwartz, J., Gillette, J. M., Manley, S., Sougrat, R., Waterman, C. M., Kanchanawong, P., and Davidson, M. W. (2009) Interferometric fluorescent super-resolution microscopy resolves 3D cellular ultrastructure. *Proc. Natl. Acad. Sci. U. S. A. 106*, 3125−3130.
(51) Pavani, S. R. P., Thompson, M. A., Biteen, J. S., Lord, S. J., Liu, N., Twieg, R. J., Piestun, R., and Moerner, W. E. (2009) Three-dimensional, single-molecule fluorescence imaging beyond the diffraction limit by using a double-helix point spread function. *Proc. Natl. Acad. Sci. U. S. A. 106*, 2995−2999.
(52) Planchon, T. A., Gao, L., Milkie, D. E., Davidson, M. W., Galbraith, J. A., Galbraith, C. G., and Betzig, E. (2011) Rapid three-dimensional isotropic imaging of living cells using Bessel beam plane illumination. *Nat. Methods 8*, 417−423.
(53) Kim, D., Jeong, K., Kwon, J. E., Park, H., Lee, S., Kim, S., and Park, S. Y. (2019) Dual-color fluorescent nanoparticles showing perfect color-specific photoswitching for bioimaging and super-resolution microscopy. *Nat. Commun. 10*, 1−10.
(54) Kisley, L., Brunetti, R., Tauzin, L. J., Shuang, B., Yi, X., Kirkeminde, A. W., Higgins, D. A., Weiss, S., and Landes, C. F. (2015) Characterization of Porous Materials by Fluorescence Correlation Spectroscopy Super-resolution Optical Fluctuation Imaging. *ACS Nano 9*, 9158−9166.
(55) Geissbuehler, S., Dellagiacoma, C., and Lasser, T. (2011) Comparison between SOFI and STORM. *Biomed. Opt. Express 2*, 408−420.
(56) Geissbuehler, S., Bocchio, N. L., Dellagiacoma, C., Berclaz, C., Leutenegger, M., and Lasser, T. (2012) Mapping molecular statistics with balanced super-resolution optical fluctuation imaging (bSOFI). *Opt. Nanoscopy. 1*, 4−7.
(57) Dertinger, T., Xu, J., Naini, O. F., Vogel, R., and Weiss, S. (2012) SOFI-based 3D superresolution sectioning with a widefield microscope. *Opt. Nanoscopy. 1*, 2−5.
(58) Dertinger, T., Colyer, R., Iyer, G., Weiss, S., and Enderlein, J. (2009) Fast, background-free, 3D super-resolution optical fluctuation imaging (SOFI). *Proc. Natl. Acad. Sci. U. S. A. 106*, 22287−22292.
(59) Moser, F., Pražák, V., Mordhorst, V., Andrade, D. M., Baker, L. A., Hagen, C., Grünewald, K., and Kaufmann, R. (2019) Cryo-SOFI enabling low-dose super-resolution correlative light and electron cryo-microscopy. *Proc. Natl. Acad. Sci. U. S. A. 116*, 4804−4809.
(60) Dertinger, T., Pallaoro, A., Braun, G., Ly, S., Laurence, T. A., and Weiss, S. (2013) Advances in superresolution optical fluctuation imaging (SOFI). *Q. Rev. Biophys. 46*, 210−221.
(61) Stein, S. C., Huss, A., Hahnel, D., Gregor, I., and Enderlein, J. (2015) Fourier interpolation stochastic optical fluctuation imaging. *Opt. Express 23*, 16154−16163.
(62) Deschout, H., Lukes, T., Sharipov, A., Szlag, D., Feletti, L., Vandenberg, W., Dedecker, P., Hofkens, J., Leutenegger, M., Lasser, T., et al. (2016) Complementarity of PALM and SOFI for super-resolution live-cell imaging of focal adhesions. *Nat. Commun. 7*, 1−11.
(63) Zhao, G., Zheng, C., Kuang, C., and Liu, X. (2017) Resolution-enhanced SOFI via structured illumination. *Opt. Lett. 42*, 3956−3959.
(64) Zou, L., Zhang, S., Wang, B., and Tan, J. (2018) High-order super-resolution optical fluctuation imaging based on low-pass denoising. *Opt. Lett. 43*, 707−710.
(65) Cox, S., Rosten, E., Monypenny, J., Jovanovic-Talisman, T., Burnette, D. T., Lippincott-Schwartz, J., Jones, G. E., and Heintzmann, R. (2012) Bayesian localization microscopy reveals nanoscale podosome dynamics. *Nat. Methods 9*, 195−200.
(66) Hu, Y. S., Nan, X., Sengupta, P., Lippincott-Schwartz, J., and Cang, H. (2013) Accelerating 3B single-molecule super-resolution microscopy with cloud computing. *Nat. Methods 10*, 96−97.
(67) Gustafsson, N., Culley, S., Ashdown, G., Owen, D. M., Pereira, P. M., and Henriques, R. (2016) Fast live-cell conventional fluorophore nanoscopy with ImageJ through super-resolution radial fluctuations. *Nat. Commun. 7*, 1−9.
(68) Oran, D., Rodriques, S. G., Gao, R., Asano, S., Skylar-Scott, M. A., Chen, F., Tillberg, P. W., Marblestone, A. H., and Boyden, E. S. (2018) 3D nanofabrication by volumetric deposition and controlled shrinkage of patterned scaffolds. *Science 362*, 1281−1285.
(69) Chen, F., Tillberg, P. W., and Boyden, E. S. (2015) Expansion microscopy. *Science 347*, 543−548.
(70) Chozinski, T. J., Halpern, A. R., Okawa, H., Kim, H. J., Tremel, G. J., Wong, R. O., and Vaughan, J. C. (2016) Expansion microscopy with conventional antibodies and fluorescent proteins. *Nat. Methods 13*, 485−488.
(71) Chang, J. B., Chen, F., Yoon, Y. G., Jung, E. E., Babcock, H., Kang, J. S., Asano, S., Suk, H. J., Pak, N., Tillberg, P. W., et al. (2017) Iterative expansion microscopy. *Nat. Methods 14*, 593−599.
(72) Gao, M., Maraspini, R., Beutel, O., Zehtabian, A., Eickholt, B., Honigmann, A., and Ewers, H. (2018) Expansion Stimulated Emission Depletion Microscopy (ExSTED). *ACS Nano 12*, 4178−4185.
(73) Li, R., Chen, X., Lin, Z., Wang, Y., and Sun, Y. (2018) Expansion enhanced nanoscopy. *Nanoscale 10*, 17552−17556.
(74) Prasher, D. C., Eckenrode, V. K., Ward, W. W., Prendergast, F. G., and Cormier, M. J. (1992) Primary structure of the Aequorea victoria green-fluorescent protein. *Gene 111*, 229−233.
(75) Chalfie, M., Tu, Y., Euskirchen, G., Ward, W. W., and Prasher, D. C. (1994) Green fluorescent protein as a marker for gene expression. *Science 263*, 802−805.
(76) Heim, R., Cubitt, A. B., and Tsien, R. Y. (1995) Improved green fluorescence. *Nature 373*, 663−664.
(77) Miyawaki, A. (2011) Proteins on the move: insights gained from fluorescent protein technologies. *Nat. Rev. Mol. Cell Biol. 12*, 656−668.

https://dx.doi.org/10.1021/acs.bioconjchem.0c00320
Bioconjugate Chem. 2020, 31, 1857−1872

(78) Chudakov, D. M., Matz, M. V., Lukyanov, S., and Lukyanov, K. A. (2010) Fluorescent proteins and their applications in imaging living cells and tissues. *Physiol. Rev. 90*, 1103−1163.
(79) Wang, S., Chen, X., Chang, L., Ding, M., Xue, R., Duan, H., and Sun, Y. (2018) GMars-T Enabling Multimodal Subdiffraction Structural and Functional Fluorescence Imaging in Live Cells. *Anal. Chem. 90*, 6626−6634.
(80) Zhang, X., Chen, X., Zeng, Z., Zhang, M., Sun, Y., Xi, P., Peng, J., and Xu, P. (2015) Development of a Reversibly Switchable Fluorescent Protein for Super-Resolution Optical Fluctuation Imaging (SOFI). *ACS Nano 9*, 2659−2667.
(81) Moeyaert, B., Nguyen Bich, N., De Zitter, E., Rocha, S., Clays, K., Mizuno, H., Van Meervelt, L., Hofkens, J., and Dedecker, P. (2014) Green-to-Red PhotoconvertibleDronpa Mutant for Multimodal Super-resolution Fluorescence Microscopy. *ACS Nano 8*, 1664−1673.
(82) Duwé, S., De Zitter, E., Gielen, V., Moeyaert, B., Vandenberg, W., Grotjohann, T., Clays, K., Jakobs, S., Van Meervelt, L., and Dedecker, P. (2015) Expression-Enhanced Fluorescent Proteins Based on Enhanced Green Fluorescent Protein for Super-resolution Microscopy. *ACS Nano 9*, 9528−9541.
(83) Zhang, M., Fu, Z., Li, C., Liu, A., Peng, D., Xue, F., He, W., Gao, S., Xu, F., Xu, D., et al. (2020) Fast Super-Resolution Imaging Technique and Immediate Early Nanostructure Capturing by a Photoconvertible Fluorescent Protein. *Nano Lett. 20*, 2197−2208.
(84) Tillberg, P. W., Chen, F., Piatkevich, K. D., Zhao, Y., Yu, C.-C. J., English, B. P., Gao, L., Martorell, A., Suk, H.-J., Yoshida, F., et al. (2016) Protein-retention expansion microscopy of cells and tissues labeled using standard fluorescent proteins and antibodies. *Nat. Biotechnol. 34*, 987−992.
(85) Lukinavicius, G., Reymond, L., D'Este, E., Masharina, A., Gottfert, F., Ta, H., Guther, A., Fournier, M., Rizzo, S., Waldmann, H., et al. (2014) Fluorogenic probes for live-cell imaging of the cytoskeleton. *Nat. Methods 11*, 731−733.
(86) Lukinavicius, G., Blaukopf, C., Pershagen, E., Schena, A., Reymond, L., Derivery, E., Gonzalez-Gaitan, M., D'Este, E., Hell, S. W., Wolfram Gerlich, D., et al. (2015) SiR-Hoechst is a far-red DNA stain for live-cell nanoscopy. *Nat. Commun. 6*, 1−7.
(87) Butkevich, A. N., Mitronova, G. Y., Sidenstein, S. C., Klocke, J. L., Kamin, D., Meineke, D. N., D'Este, E., Kraemer, P. T., Danzl, J. G., and Belov, V. N. (2016) Fluorescent Rhodamines and Fluorogenic Carbopyronines for Super-Resolution STED Microscopy in Living Cells. *Angew. Chem., Int. Ed. 55*, 3290−3294.
(88) Kolmakov, K., Hebisch, E., Wolfram, T., Nordwig, L. A., Wurm, C. A., Ta, H., Westphal, V., Belov, V. N., and Hell, S. W. (2015) Far-Red Emitting Fluorescent Dyes for Optical Nanoscopy: Fluorinated Silicon-Rhodamines (SiRF Dyes) and Phosphorylated Oxazines. *Chem. - Eur. J. 21*, 13344−13356.
(89) Lukinavicius, G., Reymond, L., Umezawa, K., Sallin, O., D'Este, E., Gottfert, F., Ta, H., Hell, S. W., Urano, Y., and Johnsson, K. (2016) Fluorogenic Probes for Multicolor Imaging in Living Cells. *J. Am. Chem. Soc. 138*, 9365−9368.
(90) Butkevich, A. N., Lukinavicius, G., D'Este, E., and Hell, S. W. (2017) Cell-Permeant Large Stokes Shift Dyes for Transfection-Free Multicolor Nanoscopy. *J. Am. Chem. Soc. 139*, 12378−12381.
(91) Grimm, J. B., Klein, T., Kopek, B. G., Shtengel, G., Hess, H. F., Sauer, M., and Lavis, L. D. (2016) Synthesis of a Far-Red Photoactivatable Silicon-Containing Rhodamine for Super-Resolution Microscopy. *Angew. Chem., Int. Ed. 55*, 1723−1727.
(92) Halabi, E. A., Thiel, Z., Trapp, N., Pinotsi, D., and Rivera-Fuentes, P. (2017) A Photoactivatable Probe for Super-Resolution Imaging of Enzymatic Activity in Live Cells. *J. Am. Chem. Soc. 139*, 13200−13207.
(93) Ye, Z., Yu, H., Yang, W., Zheng, Y., Li, N., Bian, H., Wang, Z., Liu, Q., Song, Y., Zhang, M., et al. (2019) Strategy to Lengthen the On-Time of Photochromic Rhodamine Spirolactam for Super-resolution Photoactivated Localization Microscopy. *J. Am. Chem. Soc. 141*, 6527−6536.
(94) Ye, Z., Yang, W., Wang, C., Zheng, Y., Chi, W., Liu, X., Huang, Z., Li, X., and Xiao, Y. (2019) Quaternary Piperazine-Substituted Rhodamines with Enhanced Brightness for Super-Resolution Imaging. *J. Am. Chem. Soc. 141*, 14491−14495.
(95) Macdonald, P. J., Gayda, S., Haack, R. A., Ruan, Q., Himmelsbach, R. J., and Tetin, S. Y. (2018) Rhodamine-Derived Fluorescent Dye with Inherent Blinking Behavior for Super-Resolution Imaging. *Anal. Chem. 90*, 9165−9173.
(96) Heilemann, M., Van De Linde, S., Mukherjee, A., and Sauer, M. (2009) Super-resolution imaging with small organic fluorophores. *Angew. Chem., Int. Ed. 48*, 6903−6908.
(97) Wysocki, L. M., Grimm, J. B., Tkachuk, A. N., Brown, T. A., Betzig, E., and Lavis, L. D. (2011) Facile and general synthesis of photoactivatable xanthene dyes. *Angew. Chem., Int. Ed. 50*, 11206−11209.
(98) Van de Linde, S., Löschberger, A., Klein, T., Heidbreder, M., Wolter, S., Heilemann, M., and Sauer, M. (2011) Direct stochastic optical reconstruction microscopy with standard fluorescent probes. *Nat. Protoc. 6*, 991−1009.
(99) Wijesooriya, C. S., Peterson, J. A., Shrestha, P., Gehrmann, E. J., Winter, A. H., and Smith, E. A. (2018) A Photoactivatable BODIPY Probe for Localization-Based Super-Resolution Cellular Imaging. *Angew. Chem., Int. Ed. 57*, 12685−12689.
(100) Fu, N., Xiong, Y., and Squier, T. C. (2012) Synthesis of a targeted biarsenical Cy3-Cy5 affinity probe for super-resolution fluorescence imaging. *J. Am. Chem. Soc. 134*, 18530−18533.
(101) Dertinger, T., Heilemann, M., Vogel, R., Sauer, M., and Weiss, S. (2010) Superresolution optical fluctuation imaging with organic dyes. *Angew. Chem., Int. Ed. 49*, 9441−9443.
(102) Dedecker, P., Mo, G. C., Dertinger, T., and Zhang, J. (2012) Widely accessible method for superresolution fluorescence imaging of living systems. *Proc. Natl. Acad. Sci. U. S. A. 109*, 10909−10914.
(103) Geissbuehler, S., Sharipov, A., Godinat, A., Bocchio, N. L., Sandoz, P. A., Huss, A., Jensen, N. A., Jakobs, S., Enderlein, J., Gisou van der Goot, F., et al. (2014) Live-cell multiplane three-dimensional super-resolution optical fluctuation imaging. *Nat. Commun. 5*, 1−7.
(104) Descloux, A., Grußmayer, K. S., Bostan, E., Lukes, T., Bouwens, A., Sharipov, A., Geissbuehler, S., Mahul-Mellier, A. L., Lashuel, H. A., Leutenegger, M., et al. (2018) Combined multi-plane phase retrieval and super-resolution optical fluctuation imaging for 4D cell microscopy. *Nat. Photonics 12*, 165−172.
(105) Ku, T., Swaney, J., Park, J. Y., Albanese, A., Murray, E., Cho, J. H., Park, Y. G., Mangena, V., Chen, J., and Chung, K. (2016) Multiplexed and scalable super-resolution imaging of three-dimensional protein localization in size-adjustable tissues. *Nat. Biotechnol. 34*, 973−981.
(106) Wang, Y., Yu, Z., Cahoon, C. K., Parmely, T., Thomas, N., Unruh, J. R., Slaughter, B. D., and Hawley, R. S. (2018) Combined expansion microscopy with structured illumination microscopy for analyzing protein complexes. *Nat. Protoc. 13*, 1869−1895.
(107) Cahoon, C. K., Yu, Z., Wang, Y., Guo, F., Unruh, J. R., Slaughter, B. D., and Hawley, R. S. (2017) Superresolution expansion microscopy reveals the three-dimensional organization of the Drosophila synaptonemal complex. *Proc. Natl. Acad. Sci. U. S. A. 114*, 6857−6866.
(108) Kim, D., Kim, T., Lee, J., and Shim, S. H. (2019) Amplified Expansion Stimulated Emission Depletion Microscopy. *ChemBioChem 20*, 1260−1265.
(109) Dertinger, T., Colyer, R., Vogel, R., Enderlein, J., and Weiss, S. (2010) Achieving increased resolution and more pixels with Superresolution Optical Fluctuation Imaging (SOFI). *Opt. Express 18*, 18875−18885.
(110) Van Sark, W. G., Frederix, P. L., Bol, A. A., Gerritsen, H. C., and Meijerink, A. (2002) Blueing, bleaching, and blinking of single CdSe/ZnS quantum dots. *ChemPhysChem 3*, 871−879.
(111) Nirmal, M., Dabbousi, B. O., Bawendi, M. G., Macklin, J., Trautman, J., Harris, T., and Brus, L. E. (1996) Fluorescence intermittency in single cadmium selenide nanocrystals. *Nature 383*, 802−804.

https://dx.doi.org/10.1021/acs.bioconjchem.0c00320
Bioconjugate Chem. 2020, 31, 1857−1872

(112) Hoyer, P., Staudt, T., Engelhardt, J., and Hell, S. W. (2011) Quantum dot blueing and blinking enables fluorescence nanoscopy. *Nano Lett. 11*, 245−250.
(113) Cordero, S., Carson, P., Estabrook, R., Strouse, G., and Buratto, S. (2000) Photo-activated luminescence of CdSe quantum dot monolayers. *J. Phys. Chem. B 104*, 12137−12142.
(114) Van Sark, W. G., Frederix, P. L., Van den Heuvel, D. J., Gerritsen, H. C., Bol, A. A., Van Lingen, J. N., de Mello Donega, C., and Meijerink, A. (2001) Photooxidation and photobleaching of single CdSe/ZnS quantum dots probed by room-temperature time-resolved spectroscopy. *J. Phys. Chem. B 105*, 8281−8284.
(115) Xu, J., Tehrani, K. F., and Kner, P. (2015) Multicolor 3D Super-resolution Imaging by Quantum Dot Stochastic Optical Reconstruction Microscopy. *ACS Nano 9*, 2917−2925.
(116) Yang, X., Zhanghao, K., Wang, H., Liu, Y., Wang, F., Zhang, X., Shi, K., Gao, J., Jin, D., and Xi, P. (2016) Versatile Application of Fluorescent Quantum Dot Labels in Super-resolution Fluorescence Microscopy. *ACS Photonics 3*, 1611−1618.
(117) Hanne, J., Falk, H. J., Gorlitz, F., Hoyer, P., Engelhardt, J., Sahl, S. J., and Hell, S. W. (2015) STED nanoscopy with fluorescent quantum dots. *Nat. Commun. 6*, 1−6.
(118) Ye, S., Guo, J., Song, J., and Qu, J. (2020) Achieving high-resolution of 21 nm for STED nanoscopy assisted by CdSe@ZnS quantum dots. *Appl. Phys. Lett. 116*, 041101.
(119) Lou, Q., Qu, S., Jing, P., Ji, W., Li, D., Cao, J., Zhang, H., Liu, L., Zhao, J., and Shen, D. (2015) Water-Triggered luminescent "nanobombs" based on supra-(carbon nanodots). *Adv. Mater. 27*, 1389−1394.
(120) Ge, J., Jia, Q., Liu, W., Lan, M., Zhou, B., Guo, L., Zhou, H., Zhang, H., Wang, Y., Gu, Y., et al. (2016) Carbon dots with intrinsic theranostic properties for bioimaging, red-light-triggered photodynamic/photothermal simultaneous therapy in vitro and in vivo. *Adv. Healthcare Mater. 5*, 665−675.
(121) Zhang, W., Zhu, H., Yu, S., and Yang, H. (2012) Observation of lasing emission from carbon nanodots in organic solvents. *Adv. Mater. 24*, 2263−2267.
(122) Lemenager, G., De Luca, E., Sun, Y. P., and Pompa, P. P. (2014) Super-resolution fluorescence imaging of biocompatible carbon dots. *Nanoscale 6*, 8617−8623.
(123) Chizhik, A. M., Stein, S., Dekaliuk, M. O., Battle, C., Li, W., Huss, A., Platen, M., Schaap, I. A., Gregor, I., Demchenko, A. P., et al. (2016) Super-Resolution Optical Fluctuation Bio-Imaging with Dual-Color Carbon Nanodots. *Nano Lett. 16*, 237−242.
(124) He, H., Liu, X., Li, S., Wang, X., Wang, Q., Li, J., Wang, J., Ren, H., Ge, B., Wang, S., et al. (2017) High-Density Super-Resolution Localization Imaging with Blinking Carbon Dots. *Anal. Chem. 89*, 11831−11838.
(125) Zhou, J., Sun, Y., Du, X., Xiong, L., Hu, H., and Li, F. (2010) Dual-modality in vivo imaging using rare-earth nanocrystals with near-infrared to near-infrared (NIR-to-NIR) upconversion luminescence and magnetic resonance properties. *Biomaterials 31*, 3287−3295.
(126) Xu, J., Xu, L., Wang, C., Yang, R., Zhuang, Q., Han, X., Dong, Z., Zhu, W., Peng, R., and Liu, Z. (2017) Near-infrared-triggered photodynamic therapy with multitasking upconversion nanoparticles in combination with checkpoint blockade for immunotherapy of colorectal cancer. *ACS Nano 11*, 4463−4474.
(127) Loo, J. F. C., Chien, Y. H., Yin, F., Kong, S. K., Ho, H. P., and Yong, K. T. (2019) Upconversion and downconversion nanoparticles for biophotonics and nanomedicine. *Coord. Chem. Rev. 400*, 213042.
(128) Liu, Q., Yang, T., Feng, W., and Li, F. (2012) Blue-emissive upconversion nanoparticles for low-power-excited bioimaging in vivo. *J. Am. Chem. Soc. 134*, 5390−5397.
(129) Liu, Q., Sun, Y., Yang, T., Feng, W., Li, C., and Li, F. (2011) Sub-10 nm hexagonal lanthanide-doped NaLuF4 upconversion nanocrystals for sensitive bioimaging in vivo. *J. Am. Chem. Soc. 133*, 17122−17125.
(130) Liu, D., Xu, X., Du, Y., Qin, X., Zhang, Y., Ma, C., Wen, S., Ren, W., Goldys, E. M., Piper, J. A., et al. (2016) Three-dimensional controlled growth of monodisperse sub-50 nm heterogeneous nanocrystals. *Nat. Commun. 7*, 1−8.
(131) Wang, F., Han, Y., Lim, C. S., Lu, Y., Wang, J., Xu, J., Chen, H., Zhang, C., Hong, M., and Liu, X. (2010) Simultaneous phase and size control of upconversion nanocrystals through lanthanide doping. *Nature 463*, 1061−1065.
(132) Liu, Y., Lu, Y., Yang, X., Zheng, X., Wen, S., Wang, F., Vidal, X., Zhao, J., Liu, D., Zhou, Z., et al. (2017) Amplified stimulated emission in upconversion nanoparticles for super-resolution nanoscopy. *Nature 543*, 229−233.
(133) Zhan, Q., Liu, H., Wang, B., Wu, Q., Pu, R., Zhou, C., Huang, B., Peng, X., Agren, H., and He, S. (2017) Achieving high-efficiency emission depletion nanoscopy by employing cross relaxation in upconversion nanoparticles. *Nat. Commun. 8*, 1−11.
(134) Chen, C., Wang, F., Wen, S., Su, Q. P., Wu, M. C. L., Liu, Y., Wang, B., Li, D., Shan, X., Kianinia, M., et al. (2018) Multi-photon near-infrared emission saturation nanoscopy using upconversion nanoparticles. *Nat. Commun. 9*, 1−6.
(135) Peng, X., Huang, B., Pu, R., Liu, H., Zhang, T., Widengren, J., Zhan, Q., and Agren, H. (2019) Fast upconversion super-resolution microscopy with 10 μs per pixel dwell times. *Nanoscale 11*, 1563−1569.
(136) Luo, J., Xie, Z., Lam, J. W., Cheng, L., Chen, H., Qiu, C., Kwok, H. S., Zhan, X., Liu, Y., and Zhu, D. (2001) Aggregation-induced emission of 1-methyl-1, 2, 3, 4, 5-pentaphenylsilole. *Chem. Commun.*, 1740−1741.
(137) Mei, J., Hong, Y., Lam, J. W., Qin, A., Tang, Y., and Tang, B. Z. (2014) Aggregation-induced emission: the whole is more brilliant than the parts. *Adv. Mater. 26*, 5429−5479.
(138) Mei, J., Leung, N. L., Kwok, R. T., Lam, J. W., and Tang, B. Z. (2015) Aggregation-induced emission: together we shine, united we soar! *Chem. Rev. 115*, 11718−11940.
(139) Gu, X., Zhao, E., Zhao, T., Kang, M., Gui, C., Lam, J. W., Du, S., Loy, M. M., and Tang, B. Z. (2016) A Mitochondrion-Specific Photoactivatable Fluorescence Turn-On AIE-Based Bioprobe for Localization Super-Resolution Microscope. *Adv. Mater. 28*, 5064−5071.
(140) Li, D., Qin, W., Xu, B., Qian, J., and Tang, B. Z. (2017) AIE Nanoparticles with High Stimulated Emission Depletion Efficiency and Photobleaching Resistance for Long-Term Super-Resolution Bioimaging. *Adv. Mater. 29*, 1703643.
(141) Li, D., Ni, X., Zhang, X., Liu, L., Qu, J., Ding, D., and Qian, J. (2018) Aggregation-induced emission luminogen-assisted stimulated emission depletion nanoscopy for super-resolution mitochondrial visualization in live cells. *Nano Res. 11*, 6023−6033.
(142) Fang, X., Chen, X., Li, R., Liu, Z., Chen, H., Sun, Z., Ju, B., Liu, Y., Zhang, S. X., Ding, D., et al. (2017) Multicolor Photo-Crosslinkable AIEgens toward Compact Nanodots for Subcellular Imaging and STED Nanoscopy. *Small 13*, 1702128.
(143) Wu, C., Bull, B., Szymanski, C., Christensen, K., and McNeill, J. (2008) Multicolor conjugated polymer dots for biological fluorescence imaging. *ACS Nano 2*, 2415−2423.
(144) Wu, C., Schneider, T., Zeigler, M., Yu, J., Schiro, P. G., Burnham, D. R., McNeill, J. D., and Chiu, D. T. (2010) Bioconjugation of ultrabright semiconducting polymer dots for specific cellular targeting. *J. Am. Chem. Soc. 132*, 15410−15417.
(145) Feng, L., Zhu, C., Yuan, H., Liu, L., Lv, F., and Wang, S. (2013) Conjugated polymer nanoparticles: preparation, properties, functionalization and biological applications. *Chem. Soc. Rev. 42*, 6620−6633.
(146) Wu, C., and Chiu, D. T. (2013) Highly fluorescent semiconducting polymer dots for biology and medicine. *Angew. Chem., Int. Ed. 52*, 3086−3109.
(147) Shi, H., Ma, X., Zhao, Q., Liu, B., Qu, Q., An, Z., Zhao, Y., and Huang, W. (2014) Ultrasmall phosphorescent polymer dots for ratiometric oxygen sensing and photodynamic cancer therapy. *Adv. Funct. Mater. 24*, 4823−4830.

https://dx.doi.org/10.1021/acs.bioconjchem.0c00320
Bioconjugate Chem. 2020, 31, 1857−1872

(148) Liu, J., Li, K., and Liu, B. (2015) Far-red/near-infrared conjugated polymer nanoparticles for long-term in situ monitoring of liver tumor growth. *Advanced Science. 2*, 1500008.
(149) Peng, H., and Chiu, D. T. (2015) Soft fluorescent nanomaterials for biological and biomedical imaging. *Chem. Soc. Rev. 44*, 4699−4722.
(150) Jiang, Y., and McNeill, J. (2017) Light-harvesting and amplified energy transfer in conjugated polymer nanoparticles. *Chem. Rev. 117*, 838−859.
(151) Wu, C., Hansen, S. J., Hou, Q., Yu, J., Zeigler, M., Jin, Y., Burnham, D. R., McNeill, J. D., Olson, J. M., and Chiu, D. T. (2011) Design of highly emissive polymer dot bioconjugates for in vivo tumor targeting. *Angew. Chem., Int. Ed. 50*, 3430−3434.
(152) Wu, C., Peng, H., Jiang, Y., and McNeill, J. (2006) Energy transfer mediated fluorescence from blended conjugated polymer nanoparticles. *J. Phys. Chem. B 110*, 14148−14154.
(153) Liu, Z., Sun, Z., Di, W., Qin, W., Yuan, Z., and Wu, C. (2015) Brightness calibrates particle size in single particle fluorescence imaging. *Opt. Lett. 40*, 1242−1245.
(154) Wu, C., Szymanski, C., and McNeill, J. (2006) Preparation and encapsulation of highly fluorescent conjugated polymer nanoparticles. *Langmuir 22*, 2956−2960.
(155) Sun, K., Yang, Y., Zhou, H., Yin, S., Qin, W., Yu, J., Chiu, D. T., Yuan, Z., Zhang, X., and Wu, C. (2018) Ultrabright polymer-dot transducer enabled wireless glucose monitoring via a smartphone. *ACS Nano 12*, 5176−5184.
(156) Shuhendler, A. J., Pu, K., Cui, L., Uetrecht, J. P., and Rao, J. (2014) Real-time imaging of oxidative and nitrosative stress in the liver of live animals for drug-toxicity testing. *Nat. Biotechnol. 32*, 373−380.
(157) Pu, K., Shuhendler, A. J., Jokerst, J. V., Mei, J., Gambhir, S. S., Bao, Z., and Rao, J. (2014) Semiconducting polymer nanoparticles as photoacoustic molecular imaging probes in living mice. *Nat. Nanotechnol. 9*, 233−239.
(158) Miao, Q., Xie, C., Zhen, X., Lyu, Y., Duan, H., Liu, X., Jokerst, J. V., and Pu, K. (2017) Molecular afterglow imaging with bright, biodegradable polymer nanoparticles. *Nat. Biotechnol. 35*, 1102−1110.
(159) Lyu, Y., Tian, J., Li, J., Chen, P., and Pu, K. (2018) Semiconducting polymer nanobiocatalysts for photoactivation of intracellular redox reactions. *Angew. Chem., Int. Ed. 57*, 13484−13488.
(160) Hou, W., Yuan, Y., Sun, Z., Guo, S., Dong, H., and Wu, C. (2018) Ratiometric Fluorescent Detection of Intracellular Singlet Oxygen by Semiconducting Polymer Dots. *Anal. Chem. 90*, 14629−14634.
(161) Chen, H., Wang, F., Liu, M., Qian, M., Men, X., Yao, C., Xi, L., Qin, W., Qin, G., and Wu, C. (2019) Near-Infrared Broadband Polymer-Dot Modulator with High Optical Nonlinearity for Ultrafast Pulsed Lasers. *Laser Photon. Rev. 13*, 1800326.
(162) Chang, K., Liu, Z., Fang, X., Chen, H., Men, X., Yuan, Y., Sun, K., Zhang, X., Yuan, Z., and Wu, C. (2017) Enhanced phototherapy by nanoparticle-enzyme via generation and photolysis of hydrogen peroxide. *Nano Lett. 17*, 4323−4329.
(163) Zhang, Z., Fang, X., Liu, Z., Liu, H., Chen, D., He, S., Zheng, J., Yang, B., Qin, W., and Zhang, X. (2020) Semiconducting Polymer Dots with Dual-Enhanced NIR-IIa Fluorescence for Through-Skull Mouse-Brain Imaging. *Angew. Chem., Int. Ed. 59*, 3691−3698.
(164) Yu, J., Wu, C., Sahu, S. P., Fernando, L. P., Szymanski, C., and McNeill, J. (2009) Nanoscale 3D tracking with conjugated polymer nanoparticles. *J. Am. Chem. Soc. 131*, 18410−18414.
(165) Yu, J., Song, N. W., McNeill, J. D., and Barbara, P. F. (2004) Efficient exciton quenching by hole polarons in the conjugated polymer MEH-PPV. *Isr. J. Chem. 44*, 127−132.
(166) Gesquiere, A. J., Park, S.-J., and Barbara, P. F. (2005) Hole-induced quenching of triplet and singlet excitons in conjugated polymers. *J. Am. Chem. Soc. 127*, 9556−9560.
(167) Yu, J., Wu, C., Tian, Z., and McNeill, J. (2012) Tracking of single charge carriers in a conjugated polymer nanoparticle. *Nano Lett. 12*, 1300−1306.
(168) Jiang, Y., Novoa, M., Nongnual, T., Powell, R., Bruce, T., and McNeill, J. (2017) Improved superresolution imaging using telegraph noise in organic semiconductor nanoparticles. *Nano Lett. 17*, 3896−3901.
(169) Chen, X., Li, R., Liu, Z., Sun, K., Sun, Z., Chen, D., Xu, G., Xi, P., Wu, C., and Sun, Y. (2017) Small Photoblinking Semiconductor Polymer Dots for Fluorescence Nanoscopy. *Adv. Mater. 29*, 1−7.
(170) Chen, X., Liu, Z., Li, R., Shan, C., Zeng, Z., Xue, B., Yuan, W., Mo, C., Xi, P., Wu, C., et al. (2017) Multicolor Super-resolution Fluorescence Microscopy with Blue and Carmine Small Photoblinking Polymer Dots. *ACS Nano 11*, 8084−8091.
(171) Liu, Z., Liu, J., Sun, Z., Zhang, Z., Yuan, Y., Fang, X., Wang, F., Qin, W., and Wu, C. (2019) Cooperative Blinking from Dye Ensemble Activated by Energy Transfer for Super-resolution Cellular Imaging. *Anal. Chem. 91*, 4179−4185.
(172) Sun, Z., Liu, Z., Chen, H., Li, R., Sun, Y., Chen, D., Xu, G., Liu, L., and Wu, C. (2019) Semiconducting Polymer Dots with Modulated Photoblinking for High-Order Super-Resolution Optical Fluctuation Imaging. *Adv. Opt. Mater. 7*, 1900007.
(173) Liu, Z., Liu, J., Zhang, Z., Sun, Z., Shao, X., Guo, J., Xi, L., Yuan, Z., Zhang, X., Chiu, D. T., et al. (2020) Narrow-band polymer dots with pronounced fluorescence fluctuations for dual-color super-resolution imaging. *Nanoscale 12*, 7522−7526.
(174) Jiang, Y., Hu, Q., Chen, H., Zhang, J., Chiu, D. T., and McNeill, J. D. (2020) Dual-Mode Superresolution Imaging using Charge Transfer Dynamics in Semiconducting Polymer Dots. *Angew. Chem., Int. Ed.*, 1 DOI: 10.1002/anie.202006348.
(175) Wu, Y., Ruan, H., Zhao, R., Dong, Z., Li, W., Tang, X., Yuan, J., and Fang, X. (2018) Ultrastable Fluorescent Polymer Dots for Stimulated Emission Depletion Bioimaging. *Adv. Opt. Mater. 6*, 1800333.

https://dx.doi.org/10.1021/acs.bioconjchem.0c00320
Bioconjugate Chem. 2020, 31, 1857−1872